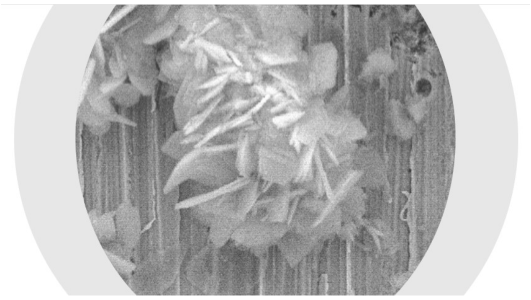

Zn Surface Engineering using new BioMOFs for localized drug delivery

Juliana Isabel Dinis Cavaco Ferreira Mota

Thesis to obtain the Master of Science Degree in

Chemical Engineering

Supervisors: Dr. Vânia André / Dr. Marta M. Alves

Examination Committee

Chairperson: Prof. Dr. Luísa Margarida Dias Ribeiro de Sousa Martins

Supervisor: Dr. Catarina Santos

Members of the Committee: Dr. Vânia André

July 2021

Declaration

I declare that this document is an original work of my authorship and that it fulfils all the requirements of the Code of Conduct and Good Practices of the Universidade de Lisboa.

Acknowledgements

Em primeiro lugar queria agradecer às minhas orientadoras, Dr.ª Vânia André e Dr.ª Marta Alves pela disponibilidade, atenção, supervisão e conhecimentos transmitidos nos últimos meses. Desde o dia da primeira reunião, que nunca vou esquecer, obrigada por me terem ajudado a concretizar um sonho!

A todo o grupo de trabalho do projeto ACFs Dr.ª Paula Alves, Catarina Bravo quero agradecer a ajuda no desenvolvimento deste trabalho, e restantes colegas pelo apoio nos últimos meses.

À Professora Dr.ª Maria Teresa Duarte agradeço pela integração no seu laboratório e por todo o conhecimento transmitido.

A todos os colegas do laboratório de corrosão quero agradecer o apoio, suporte e forma como fui recebida de braços abertos por todos.

À Professora Dr.ª Maria de Fátima Montemor quero agradecer todos os conselhos e sugestões transmitidos ao longo do desenvolvimento do trabalho.

Ao Professor Dr. João Salvador Fernandes agradeço todos os conhecimentos transmitidos no decorrer do projeto.

Ao Dr. Auguste Fernandes agradeço pela caracterização térmica TGA/DSC.

À Professora Patrícia Rijo docente na Universidade Lusófona e investigadora nos centros de investigação CBIOS e iMed-ULisboa, pelos ensaios de microbiologia.

A duas professoras que me marcaram de uma forma especial neste caminho Professora Ana Paula Soares Dias e Professora Maria das Mercedes Esquível

Agradeço ao Centro de Química Estrutural do Instituto Superior Técnico.

Agradeço também o financiamento pela FCT (UIDB/00100/2020, UIDP/00100/2020) and PTDC/QUI-OUT/30988/2017) e FEDER, Portugal 2020 and Lisboa2020 (projeto LISBOA-01-0145-FEDER-030988), assim como projetos que financiaram o trabalho e que permitiram o acesso a equipamentos e reagentes.

Aos colegas de curso em especial Ana, Karina, Inês muito mais que colegas, amigas; aos "improváveis" GDC, Mariana, Albertina, Joana e Ângelo mal nos conhecíamos, mas desde o primeiro dia estiveram lá e de que forma.

À minha família pelo apoio incondicional. Aos "amigos-família" Sara, Artur, Ana "do Porto ". Aos meus mais que tudo, os meus afilhados B e ZT.

Ao Tiago pela paciência em dia menos bons, por estares sempre lá e por sempre acreditares em mim.

Ao Zeca, não há palavras que descrevam tudo o que fizeste.

Abstract

Antibiotic resistance is a well-acknowledged problem worldwide, that directly or indirectly impacts different areas of healthcare intervention. This, allied to a society where the average life expectancy tends to increase, presents a great challenge to our healthcare systems. In such ageing societies, bone restorations are particularly frequent, and whenever a surgical intervention is required, the risk for infections greatly increases in this fragile segment of our population. Therefore, it is of utmost importance to guarantee the success of these medical interventions, a strategy that can be achieved by using innovative systems for bone-healing, by using resorbable implants to avoid a second surgery for implant removal upon healing, allied to functionalization with novel antimicrobial drugs.

The production of new drugs is a time-consuming area of research with associated large investments, including in the extremely difficult step of the molecular structure validation of the newly synthesized drugs. Therefore, the use of already known antibiotics to create new structures as antibiotic coordination frameworks (ACFs), as presented in this thesis, are expedite strategies that can accelerate these drugs acceptance and entrance into the pharmaceutical markets. Moreover, the new ACF structures reported in this thesis were synthesized by mechanochemistry, an elected green method route that not only is environmentally friendly but is also safer when aiming at human health applications.

The use of these new structures, as functional coatings on bioresorbable implant materials, represents the state-of-the-art in ensuring the success of transient bone-healing applications. Due to its well-accepted biocompatibility and degradation properties, zinc was chosen as the material to be functionalized with newly synthesized antibacterial AFCs.

To ensure the use of green and safe methodologies, while preserving the ACF chemical integrity, electrophoresis was used for the ACF coating formulations on zinc. Despite the electrochemical modification of zinc during the coating formulation, the work presented herein proved the potential of this strategy to answer the demand for new antibacterial materials in bone implant applications.

To characterize and ensure ACFs stability, deep physicochemical analyses were performed along with the design of the materials, namely by x-ray diffraction, thermal analysis, scanning electron microscopy, energy dispersive spectroscopy, among others. Moreover, the influence of ACF coatings on this biomaterial degradation was studied by advanced electrochemical techniques.

The results attained were discussed, presented in two conferences as a poster and selected oral presentation, and future research strategies proposed.

Keywords: *antibiotic coordination framework, calcium, electrophoresis,* implant, *mechanochemistry, zinc*

Contents

List of tables

List of figures

List of abbreviations

AC, Alternating Current

ACF, Antibiotic Coordination Framework,

ACF1, Antibiotic Coordination Framework, coordination between nalidixic acid, salicylic acid and calcium.

ACF2, Antibiotic Coordination Framework, coordination between nalidixic acid, nicotinic acid and calcium.

ACF3, Antibiotic Coordination Framework, coordination between nalidixic acid, isonicotinic acid and calcium

API, Active Pharmaceutical Ingredient

BioMOF, Biodegradable therapeutic Metal-Organic Framework

CPO, Coordination Oslo Polymer

DSC, Differential Scanning Calorimetry

EBSD, Electron BackScatter Diffraction

EDS, Energy Dispersive Spectroscopy

EIS, Electrochemical Impedance Spectroscopy

EMA, European Medicines Agency

FDA, Food and Drug Administration

ILAG, Ion-and Liquid-Assisted Grinding

LAG, liquid-assisted grinding

MIL, Materials of Institute Lavoisier

MOF, Metal-Organic Frameworks

n.d., not determined

NG, Neat-Grinding

POLAG, Polymer-Assisted Grinding

PXRD, Powder X-ray Diffraction

SBF, Simulated Body Fluid

SCXRD, Single-Crystal X-ray Diffraction

SEM, Scanning Electron Microscope

TG or TGA, Thermogravimetry or Thermogravimetric Analysis

XRD, X-ray Diffraction

A LITERATURE REVIEW

1 Introduction

The economic, social and cultural development of a country and a community is inevitably related to the scientific and technological R&D. Scientists discover answers to societal challenges and improvements to the existing systems for better performances. Bone implants represent one of the systems that require huge efforts to improve their efficacy, especially in an era where bacterial infections, due to the worldwide increasing resistance to antibiotics, can jeopardize these essential medical interventions.

For instance, in trauma-related bone reconstructions, fracture-related infections associated with osteosynthetic stabilization are a major problem as the surgery field is often contaminated due to bacterial access through open wounds. This leads to an infection risk ranging from 10% to 50% depending on the fracture type. Thus, implant-related bone infections are a serious burden in current and future health care with clinical trials showing that bacterial infection is one of the most important causes of implants failure(1).

1.1 Bone

The function of bone has the main purpose of structural support, protection, storage of healing cells and minerals, essential for ions homeostasis. Human bones in general are a combination of various materials structures at different scales. Bone architecture is a hierarchical and highly complex structure divide by scale in macrostructure, microstructure, sub-microstructure, nanostructure and sub-nanostructure (Figure 1).

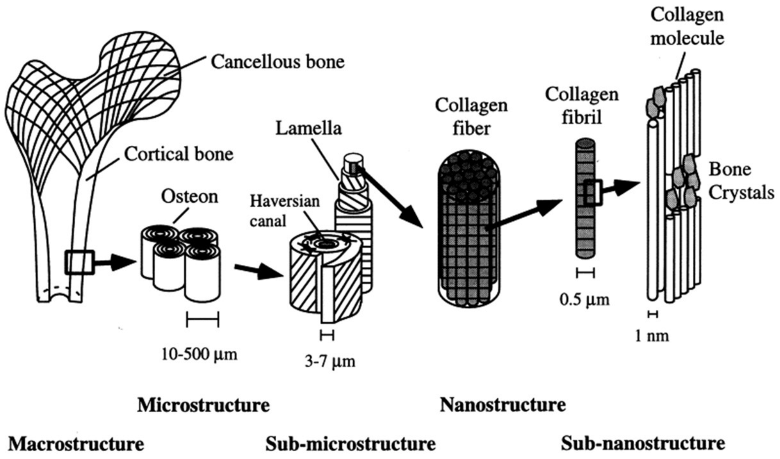

Figure 1: Hierarchical structural organization of bone(taken from (2))

Macrostructure is composed of two different bone types, cancellous and cortical, with different properties; microstructure, between 10 to 500 µm, contains Haversian systems, osteons, single trabeculae; sub-microstructure, between 1 to 10 µm, lamellae; nanostructure, between ± 500 nm to 1 µm, includes fibrillar collagen and embedded mineral; sub-nanostructure, <500 nm, as the molecular structure of constituent elements, such as minerals, collagen, and non-collagenous organic proteins. Bone is an irregular, non-homogeneous and anisotropic material (2). Mechanical properties (Table 1), evaluated by the response of a material to applied external forces, are essential in bone-healing processes.

Table 1: Mechanical properties of cortical bone, cancellous bone(2)

Material	Density (g/cm^3)	Yield strength (MPa)	Ultimate tensile strength (MPa)	Young Modulus (GPa)
Cortical bone	1.8 – 2.0	104.9–114.3	35 – 283	5 - 23
Cancellous bone	1.0 – 1.4	-	1.5 – 38	0.01 – 1.57

When dealing with implanted materials, it is important to bear in mind that interaction between this and the newly formed tissues will occur and will be modulated by each other response along the time. This is particularly relevant during bone regeneration as it is composed of four steps. "The first manifestation is inflammatory response, leading to signaling to stem cells, which will differentiate into chondrocytes that will produce cartilage and osteoblasts, responsible for constructing a new bone. After the already formed cartilaginous matrix, it will be mineralized, and then it will be resorbed forming the bone. This formation generates the primary bone, which undergoes a remodeling of the preformed bone callus, occurring a second resorption, which restores the anatomical structure"(3).

When the development of the studies is to fine-tune a biomaterial for bone healing, is important that this material provides osteoconductive, osteoinductive properties (Figure 2), or even an osteogenic environment(4). Osteoinduction is a process that occurs regularly in any type of bone healing process. Involves the recruitment of immature cells and their stimulation to develop into preosteoblasts. Osteoinduction is responsible for the majority of the bone healing process in situations such as bone fractures. Osteoconduction which means that bone grows on a surface, is regularly seen in the case of bone implants. Implant materials of low biocompatibility such as copper, silver (as coating material) and bone cement show little or no osteoconduction. Osteointegration is the link of an implant achieved by direct bone-to-implant contact(5).

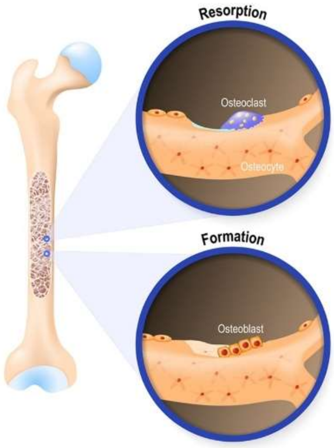

Figure 2: Remodeling process bone: osteoblast and osteoclast. *(taken from (6))*

Overall, the new biomaterial is required to have bone compatibility, strength, and must promote bone regeneration on the affected area(7, 8). Whatsoever, this can be jeopardized when bacteria, instead of preosteoblasts, adhere to the implanted material, compromising the effectiveness of the surgical procedure, and in more severe cases can be even life-threatening.

As such, the discovery and development of new and improved drug systems are of utmost importance to ensure the success of this and other medical interventions.

1.2 Active Pharmaceutical Ingredients

Quoting the philosopher De Voltaire, ”Les médecins administrent des médicaments dont ils savent très peu, à des malades dont ils savent moins, pour guérir des maladies dont ils ne savent rien” (1694)(9), meaning that doctors administer drugs of which they know so little, to patients of whom they know less, to cure diseases of which they know nothing. Even though this might have been reasonable in 1694, science evolved hugely, and important developments have been made since then, which allowed us to know much more nowadays about the diseases and how to cure them, which has a major positive impact on society. In fact, since the beginning of healing times through drugs, in which active ingredients were obtained from plants, until the industrialization of pharmaceuticals, in 1898, when the first drug, Aspirin® was discovered by Félix Hoffman(10), there has been a remarkable evolution that is still in continuous development.

Drugs are undoubtedly fundamental for health systems worldwide, as they are an effective way to reduce the burden of diseases and mortality, promoting longer life expectancy and improvement of life’s quality. Nevertheless, there is still a lot of space for improvement and optimization. For example, there are often issues associated with the use of a specific active pharmaceutical ingredient in pharmaceutical formulations, derived from their low solubility, low bioavailability, low stability, or inadequate properties for the formulation that might interfere with their biological performance(11-13).

Nowadays it is well established that an Active Pharmaceutical Ingredient, API, can be considered any type of substance or combination of them used in a finished pharmaceutical product, intended to provide pharmacological activity. Such substances are supposed to supply drugs’ activity or alternatively have direct effects on the diagnosis, cure, mitigation, and treatment. Also, APIs can a have direct effect in restoring, correcting or modifying physiological functions in human beings(14-16). Usually, APIs are present in small dosages within the drug formulations.

The structure of API incorporates a vital impact on the effectiveness of a drug, producing the desired results, and in the safety profile of the drugs. Poorly manufactured or compromised APIs are connected to serious problems, like illness or even death(17). The importance of such types of compounds implies the need for verification. The validation and control of new drugs are made by the European Medicines Agency (EMA), at an European level, and by Food and Drug Administration (FDA), throughout America(18, 19). In terms of intrinsic value, APIs are amongst the most valuable materials on the planet(20), and therefore a lot of investment, both in industry and academia, is put into R&D related to APIs and drug design, not only to discover new molecules but also to find alternative pathways to improve the efficiency of the currently available ones.

Antibiotics are amongst the classes of APIs that have been recently demanding urgent innovation.

1.3 Antibiotics

Since the 1940s, antibiotics have been used as effective treatments against bacterial infections. They have a strong and powerful capability to defeat diseases caused by bacteria, therefore saving lives. When used appropriately, these can quickly and effectively eliminate infections and prevent their growth within a few days, helping patients to restore their normal activity(21, 22).

From the perspective of antibiotics effectiveness, it is possible to identify highly effective drugs that can cure numerous infections, from the simpler to the more problematic and difficult cases. An infection can occur at any body location and can be initiated by the microorganism itself or by the body's response to its presence. Bacterial infections can be, for instance, a consequence of surgeries, in which various instruments are used, and incisions are made, enhancing the possibilities for microorganisms' proliferation(23). Despite that medicine has evolved in the discovery of antibiotics, the existence of bacterial resistance has been also identified (Figure 3).

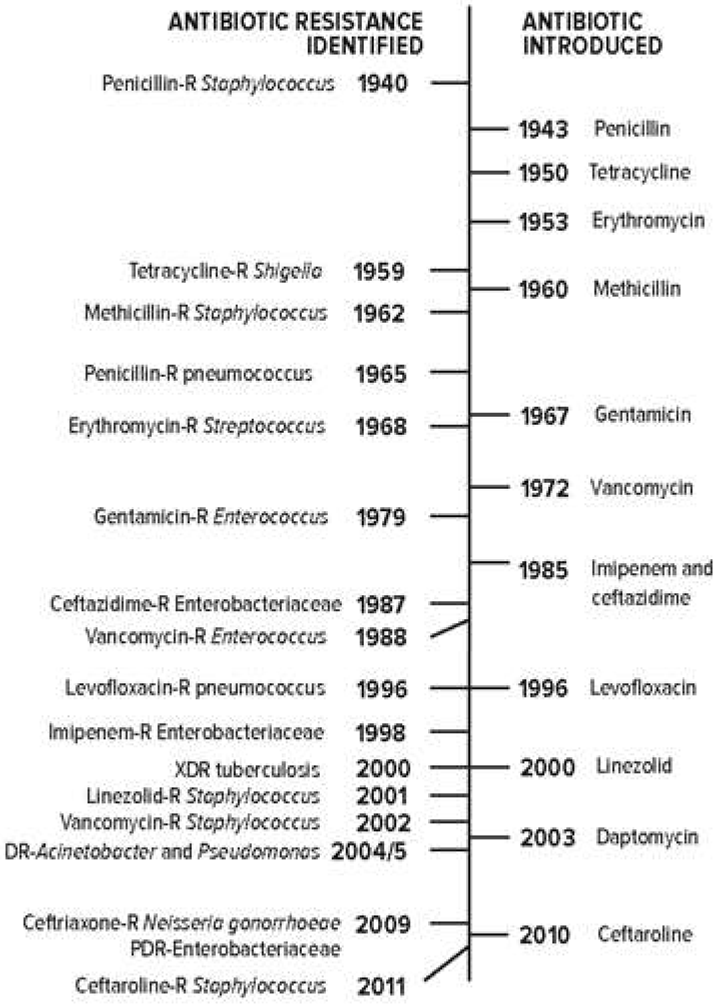

Figure 3: Timeline of key events in developing antibiotic resistance (taken from (24)), where PDR - pan-drug-resistant, R – resistant, XDR- extensively drug-resistant. Note: penicillin was in limited use before widespread population usage in 1943

Moreover, bacteria that are commonly present in the human body without causing disease, for example, *Staphylococcus aureus* that exist at the surface of the skin, intestines and urinary tract, may also be responsible for infections. Even though this type of bacteria is easily destroyed by disinfectants, soaps and high temperatures, they are transported from person to person by direct or indirect contact and can easily be transmitted from harmless (external body) to harmful (internal body) zones(25, 26).

The accomplishment of antibiotics was also recognized in cases of progressing diseases, reducing the chances of severe infections and associated complications(22).

Despite all the benefits, one of the most well-known problems associated with antibiotics is the fact that some bacteria developed resistance mechanisms to the drugs, making most of the currently available antibiotics ineffective. This efficiency is being beaten by one of the biggest health problems in the world, the resistance to antibiotics(27). Once bacteria develop resistance mechanisms, it can lead to severe health issues in the future, if not properly treated, with impact also at an economical level(28). This problem can inclusively jeopardize most types of surgeries, such as pacemakers' implants, childbirths, bone replacement or even plastic surgery, as infectious diseases commonly arise as complications in these cases.

The growing number of multidrug-resistant bacteria is a global health problem that threatens the effective prevention and therapy of bacterial infections(23, 29), possibly leading to a point of inversion of the benefits of the use of antibiotics(28, 30, 31). This can induce major problems in a not-so-distant future: it is expected that by 2050 infections due to resistant bacteria become the leading cause of death, overpassing cancer cases(32).

Currently, as synthetic antibiotics, quinolones have very important anti-infectious characteristics(33), being applied in the treatment of various infections(34). These have also been reported as having antitumor, anticancer and antiviral activities(35-37). Their adequate absorption and bioavailability(38, 39), related to their structure make this group of drugs of great interest for research. The presence of carboxylic acid and carboxyl groups are important for hydrogen bonding, and the additional group connected (R_1) to the nitrogen atom interfere with microbiological functions and so with important properties such as the pharmacokinetic of the compound. The antibacterial potency was directly associated with the substituent (R_2) where H or small rings at this position favor the activity, and the efficiency against Gram-positive bacteria was controlled by the substituent at position (R_5), while the facility of cell penetration is dependent on the substituent (R_6) and the has a significant influence on potency, spectrum, safety and pharmacokinetics (R_7) (Figure 4).

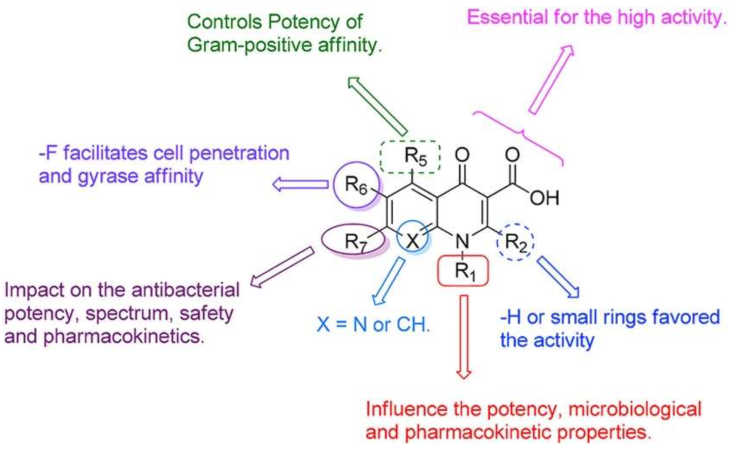

Figure 4: The structure– antibacterial activity relationship of quinolones(40)

Nalidixic acid is a first-generation quinolone antibiotic (Figure 5), mainly used against urinary tract infections caused by *Escherichia coli* and other pathogenic Gram-negative bacteria(41), being less effective in Gram-positive bacteria. One of the aspects that led to the decline in the use of this antibiotic is its poor solubility, thus reducing its potential in the pharmaceutical industry(12, 42). This API has been studied with the purpose to produce alternative structures, that can be advantageous in terms of physicochemical properties as well as antimicrobial activity(13, 43).

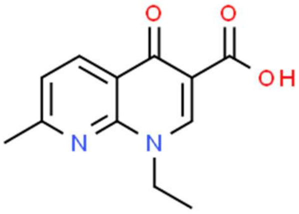

Figure 5: Chemical structure of nalidixic acid

One option that has been explored to give rise to these new forms is based on the ability of quinolone antibiotics to coordinate to biocompatible metals, such as sodium and potassium (group 1)(44), magnesium and calcium (group 2)(13, 44, 45), vanadium (group 5)(46), manganese (group 7)(13, 45, 47), cobalt (group 9) (48, 49), cooper and silver (group 11)(50, 51), zinc (group 12)(12, 45) and bismuth (group 15)(52).

These new structures show improvements in terms of biological and pharmaceutical activities, in comparison with the corresponding free drug(53, 54). Furthermore, to this very important improvement, some of the new structures also present an enriched level of chemical composition, polar, electrical, acidic and redox properties(55-57).

This approach to develop new forms of already available APIs, which consists of using antibiotics as ligands for the formation of coordination compounds and metal-organic frameworks, as ACFs, is a promising pathway to re-design antibiotics with improved physicochemical properties and augmented antimicrobial activity. Ultimately these new forms may be useful to overcome the growing trend of bacterial resistance, linked with high costs of research and development of new APIs come to be a huge advantage of being based on already authorized molecules.

1.4 Metal-Organic Frameworks

Studies on metal-organic frameworks (MOFs) started in 1954 and these systems have been used for many different applications over the last decades. Some of these applications include the pharmaceutical fields, with the use of MOFs with bio-friendly composition as drug carriers being proposed to surpass some of the problems presented by the most common systems used for drug delivery. The Coordination Oslo Polymer (CPO) and the Materials of Institute Lavoisier (MIL) were the first families of MOFs considered as potential drug delivery systems. In both cases, the strategy consisted of building an adequate three-dimensional network with large channels available for drug encapsulation.

This strategy is simple and highly effective in improving the drug transport capacity. The ability of CPO-27-Mg (as ligand 2,5-dihydroxyterephthalic acid, with one-dimensional pores) to encapsulate *Aspirin*® (8% by weight) and

Paracetamol® (14% by weight) has been demonstrated (Figure 6a) (58). MIL-100 (Figure 6b) and MIL-101, with a center metal with chromium, were studied for the encapsulation and release of *Ibuprofen*®, reaching different concentration values in both structures (0.347 g of ibuprofen / g MOF for MIL-100 and 1.376 g of ibuprofen / g MOF to MIL-101), justified by the difference in their compositions and the different crystal structures(59).

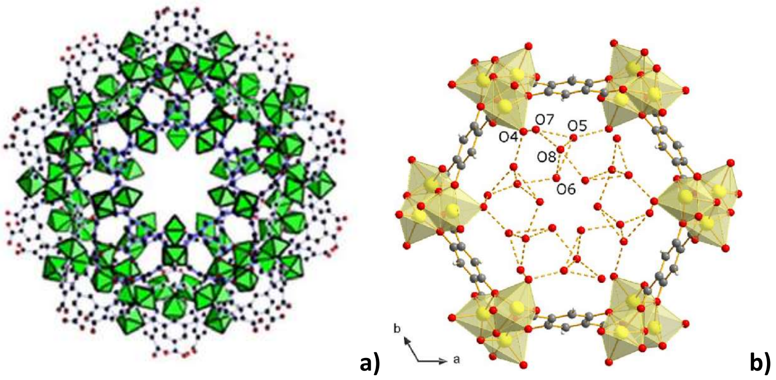

Figure 6: a) Excerpt of the crystal structure of CPO-27-Mg(taken from (60)*) b)Structure of MIL-100(Cr) depicting the small cages (taken from*(59)*)*

An evolution of this system was the biodegradable therapeutic MOF called bio-MOF-1 (Figure 7), This is a particular case of zinc-adeninate coordination, interconnected with biphenyldicarboxylic acid ligand, which presents a three-dimensional porous metal-organic structure, being a material with great potential as a drug release system, due to its non-toxic components and biocompatible properties. The loading of different drugs into this porous structure has already been reported, and the release of the bioactive molecules has been studied, showing promising results(61).

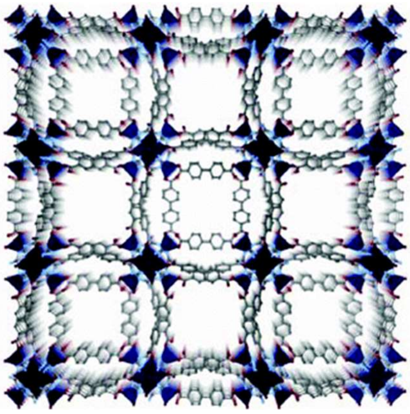

Figure 7: Crystal structure of bio-MOF-1 consists of zinc–adeninate columns linked together into a 3-D framework by biphenyldicarboxylate linkers to generate a material with 1-D channels along the c crystallographic direction (taken from (61))

The use of commercially available active pharmaceutical ingredients as organic ligands for the formation of such networks does not require the existence of pores, while presenting some advantages, namely, the elimination of adverse effects subsequent from the degradation of the network with the release of a non-active ligand(62). Where started to be used the designation of BioMOF, as a designation of biodegradable therapeutic Metal-Organic Framework.

Following this approach, several BioMOFs and antibiotic coordination frameworks (ACFs), when was used an antibiotic, have been reported(52,63,65). These new crystalline structures have improved physicochemical properties, particularly in their solubility. The solubility of a drug is a determining factor for its ability of absorption and for a suitable bioavailability(66, 67). The antimicrobial activity of the new compounds was also evaluated, often showing an increase when compared to the starting antibiotics (13, 48, 67, 68).

The work presented herein is focused on the developments of ACFs enclosing nalidixic acid, as a ligand. Nalidixic acid is an antibiotic, normally administered orally, and it is used for the treatment of urinary tract infections against Gram-negative bacteria, such as E. coli, Enterobacter, Klebsiella, and Proteus species(12, 13, 43, 50, 69). The possibility of combining into the new structures compounds with therapeutic advantages led to the use of salicylic, nicotinic and isonicotinic acids as second ligands. Salicylic acid is an anti-inflammatory agent and it has been reported also as a topical antibacterial agent(70). Nicotinic acid, usually known as vitamin B3, is used to prevent and treat niacin deficiency, as a vitamin, nicotinic acid helps to support the body's ability to make and break down natural compounds needed for good health(71). Isonicotinic acid causes disruption of the bacterial cell wall and loss of acid-fast properties in vulnerable mycobacteria, leading to bactericidal properties against actively growing intracellular and extracellular susceptible mycobacteria(72, 73).

When designing BioMOFs and ACFs, the choice of the metal is also a vital step. Although the coordination of APIs to several metals, from several groups of the periodic table, has already been reported, their selection needs to be conscious. Calcium is the fifth most abundant element in the human body, with more than 99% found in the bone skeleton, and in less extent, calcium can also be found in cells (especially muscle’s cells) and the blood. Calcium performs important functions such as: participating in the normal functioning of various enzymes, blood clotting, heart rate, and muscle contractures (74-76). Matching to the presented characteristics as well as the main purpose of this work, application in bio-implants, calcium was the chosen metal for this case study as a vital mineral used to favor bone healing processes.

After defining the design of new compounds, it is necessary to define the most appropriate synthetic methods.

1.4.1 Synthetic Methods

This type of material is traditionally synthesized by solution methods, in particular, by hydrothermal and solvothermal synthesis, which require the use of solvents, temperature and several hours/days to reach the desired products(77). Recently, other synthetic approaches, as microwave synthesis and mechanochemistry, have been successfully explored. Mechanochemistry is an environmentally friendly technique, which leads to a massive reduction in the use of solvents. Mechanochemistry driving force was correlated with the energy produced by the impact applied on the reactants such as using a mortar and pestle or resulting from the impact on ball mills.

The successful use of this technique for the synthesis of MOF is known and reported(45, 51, 79, 80). A relevant aspect of this technique is the elimination or very small use of solvent. Also, other significant advantages over traditional techniques should be highlighted, such as the reduction of reaction time and temperature (normally occurs at room temperature), the easiness of operation, high yield of reactions and purity of the compounds(81, 82).

Mechanochemistry can occur with some variations such as a) grinding without any addition of solvent(NG, neat-grinding); b) grinding with the addition of catalytic amounts of solvent (LAG, liquid-assisted grinding); c) grinding with catalytic amounts of solvent and an ionic salt (ILAG, ion-and liquid-assisted grinding); and d) grinding using catalytic amounts of polymers (POLAG, polymer-assisted grinding)(78-80, 83, 82).

The grinding process can be done using a manual approach, in which a mortar and a pestle are used, or it can make use of different mills, such as horizontal vibration ball mills. At an industrial plant, the process can occur on ball mills, in which a "rather large number of grinding bodies and the material being ground are placed inside a cylinder rotating around its central axis. Due to forces of friction between the cylinder walls and the milling bodies, the bodies start to move and grind the raw material. Sometimes grinding bodies are not used, and particles of the material grind themselves. This process is known as "auto-grinding". An example of industrial equipment is given in Figure 8(85).

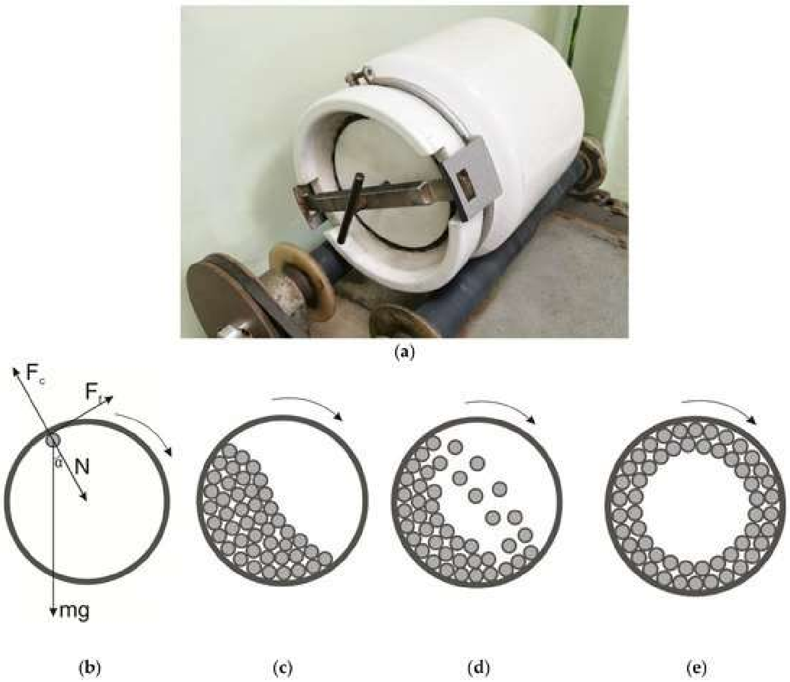

Figure 8: A real-world example (a), the effect of forces (b) and the types of motion of grinding bodies in a ball mill: (c)—rolling over; (d)—falling; (e)—rolling (taken from(85))

1.5 Drug delivery

In pharmacology, we can identify several routes of administration of drugs. The methods used are typically oral, by injection (parenteral administration), rectal, vaginal, ocular, nasal, inhalation, nebulization, cutaneous, and transdermal. The chosen method is directly dependent on the substance that the patient must be administrated with (86, 87).

Identified by their facility and convenience, the most commonly used method is the oral route (88). This route can sometimes lead to high administration doses to achieve and maintain an effective concentration at the target point, which can result in toxicity, gastrointestinal intolerance and resistance to medicines. Derivative the nonlinearity of the concentration-effect relationship, administration of the different doses and routes is expected to produce different outcomes, which is a very crucial variable for oral drug delivery (89). In addition, a well-known problem, some API exhibits poor aqueous solubility that poses a major problem in their oral administration, getting further complicated due to their short bioavailability and inconsistent absorption(90, 91). To mitigate these problems, local drug delivery by its inherent characteristic can decrease the drug concentration used and eliminate solubility problems, moreover, this administration route has the advantage to be administrated on a specific location, without the need to 'travel' throughout the organism. This strategy can decrease costs, as minimal concentrations will be required and the associated side effects(92). The challenge of this administration route lies in the capability to reach the desired location.

A particular method to applied local drug delivery is by loading implantable devices with the desired drug. This can be achieved by coating and/or functionalizing the implantable biomaterial with the new designed ACFs.

1.6 Biomaterials for Implant Applications

Biomaterials have the implicit property of interact with biological systems such as proteins, cells, tissues, organs and organ systems in order to treat, expand or replace body tissues, organs or functions. According to their origin, these can be natural, synthetic or a mixture of both(8, 93). The type of biomaterials, available in different forms and structures are expected to actively interact with the body when included in the affected areas (94).

In the last decades, the biomaterials' field had great advances, and nowadays a variety of materials are used on bioimplants, which can go from ceramic, glasses, polymers composites, glass-ceramics to metal alloys. Many properties such as the mechanical properties, toxicity, surface modification, degradation rate, biocompatibility, corrosion rate and scaffold design are taken into consideration (95, 96).

Following the evolution of biomaterials was possible to identify three generations: the first generation refers to bio inert materials, mainly metals and alloys focus on not causing foreign body reactions in the organism; the second generation involves bioactive materials, which have the ability to interact with biological tissue, creating bioadhesion; herein are also included the biodegradable materials, which can gradually disappear upon being introduced into the body; the third generation is made up of responsive materials able to stimulate cellular responses at molecular levels (biomimetics – biological structure and tissue engineering)(97).

Within the biodegradable materials, some have been designed to degrade and be resorbed inside the body. These types of implants are known as bioabsorbable implants.

1.7 Bioabsorbable Implants

Bioabsorbable implants are materials that will be slowly replaced by the newly formed tissues, as these degrade along the time while will be simultaneously reabsorption *in vivo*. As such, the implanted material will be eliminated by specific metabolic pathways(98-100). Moreover, this metabolic interaction can result in positive tissue restoration, for instance by stimulating bone formation.

Medical devices presents alternatives to bone implants, such as synthetic biomaterials, whose applicability has several advantages that can range from not causing damage to healthy tissues, low risk of viral and bacterial contamination, to easy and affordable access to the product (7, 101, 102).

Most of these devices, temporary implants, can be polymeric or metal-based materials, however, metallic materials like iron, zinc and magnesium have been reported to be the most promising ones, especially for load-bearing applications as in bones (Figure 9) (103).

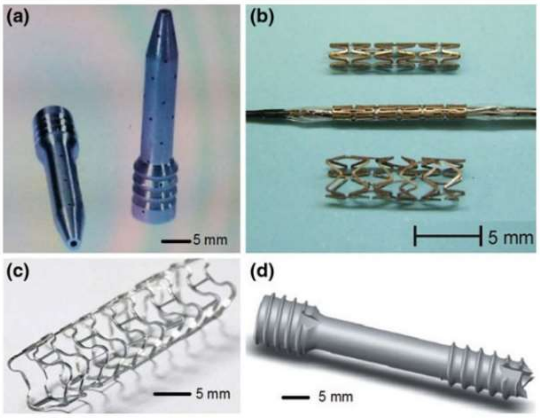

Figure 9: Biodegradable metals implants, a) Magnesium alloy cross pin, b) Iron alloy stent, c) Magnesium alloy stent d) Magnesium alloy compression screw (taken from (104))

The use of bioabsorbable implants in orthopedic surgical procedures is increasingly frequent, as by avoiding a second surgery for the implant removal will naturally decrease the risk of developing associated implant infections. Nevertheless, there have been some reports where bioabsorbable materials were removed, which lead to the unwanted second surgery for implant removal(105, 106). As expected, the degradation rate occurs gradually throughout time until the healing process is completed; however, iron implants were reported to have a very slow degradation rate, at the opposite side, magnesium implants had a higher degradation than that required for a complete healing process. Moreover, upon degradation, magnesium releases hydrogen a reaction that can inhibit this metal used in clinical applications(107). Zinc has a degradation behavior between iron and magnesium, presenting a corrosion rate that matches the required for bone-healing applications(108).

1.7.1 Zinc implants

As a biodegradable material, zinc can be used porous bone implants, to support, nourish, and stimulate regeneration of damaged blood vessels and new bone formation(108).

The density of zinc is higher than that of bones. Despite this miss-match, which is not a concern for bioresorbable materials as the stress-shielding will be minimal, the maximum stress that zinc can withstand, while being stretched or pulled before breaking, is between the value for cortical bone and higher for cancellous bone. A global view of young modulus, elasticity, reveals that zinc has a major elasticity than both types of bones (Table 2). Ideally, the best material would be that with mechanical properties as close as that of bone, whatsoever, there is still a long way to go to find a material with such properties, like magnesium, that possess an adequate degradation rate, like that reported for zinc.

Table 2: Mechanical properties of zinc (109)

Material	**Density (g/cm^3)**	**Yield strength (MPa)**	**Ultimate tensile strength (MPa)**	**Young Modulus (GPa)**
Zinc	7.10	-	90	95

To potentiate the use of zinc as a biomaterial for implantable devices, different and improved properties are required (110). Besides being a biocompatible metal, the material itself and the resulting corrosion products are innocuous (111). These are typically ZnO, $Zn(OH)_2$, and $Zn_3(PO4)_2$(112-114). When in the presence of calcium ions (as in body fluids), these can react with phosphate and precipitate in the form of calcium phosphate or Zn-doped calcium phosphates(115-118). If chloride (also present in body fluids), reacts with zinc, $Zn_5(OH)_8Cl_2$ will be formed instead(119).

Zn(II), as a micronutrient(111), is present in human cells, where it has several functions, including in immune system regulation (120). Its daily intake is 4 to 14 mg/day and dietary obtaining from meat, seafood, cereals, nuts, eggs, grains, legumes, and milk. The presence of zinc in the body is identified by its concentration in plasma, where normal levels are established between 70 and 120 µg/dL (121). Zinc deficiency has more relevant physiological effects than toxicity, as low zinc values can cause growth retardation(122). The importance of Zn in bone metabolism is evident, therefore, its use as an implantable material with endowed antimicrobial properties can ensure success in bone-healing applications.

1.8 Antibacterial Coatings Design

There are several types of coatings used in bioresorbable implant applications with antibacterial properties. These can be organic, inorganic or even hybrid coatings. Depending on the purpose of these coatings, different formulations can be prepared. While for magnesium these are typically designed to delay the corrosion onset, for iron, these are targeted for an accelerated corrosion onset. For zinc, the corrosion rate should ideally be kept, as such coatings are meant to deliver exclusively antimicrobial properties to the material without influencing the corrosion onset.

For that purpose, several techniques can be used for instance, spin-coating or dip-coating, typically used with polymer and sol-gel coatings (123, 124); layer-by-layer assembly, where films are formed by depositing alternating layers (125); electrophoretic deposition, a two-step process by which the particles suspended in a colloid solution are collected onto a conductive substrate; chemical vapor deposition, a coating process that uses thermally induced chemical reactions at the surface of a heated substrate(126); pulsed laser deposition, high-power pulsed laser beam is focused inside a vacuum chamber to strike a target of the material that is to be deposited among others (127).

In almost all of the techniques presented, high temperatures or secondary compounds (mostly dangerous for human heath) or combinations of these are necessary. In a coating process intended for medical applications, where drugs are used in their formulation, it is extremely important to preserve the drug structure and its chemical integrity. When using conductive substrates, like zinc, a technique requiring few or no additives that satisfy the purpose of coating medical implants is electrophoresis.

1.8.1 Electrophoresis deposition

Based on the produced ACFs that have associated a specific global charge (positive or negative), the drug deposition on the metal is based on the movement and deposition of the molecules under an electric field on the conductive substrate (Figure 10). Depending on the conditions used (applied voltage/current, time and electrolyte) thin or thick films and coatings can be produced. This process can be applied for the design of coatings with a wide range of materials, as fine powders or colloidal particles of metals, ceramics, polymers, and composites (128, 129).

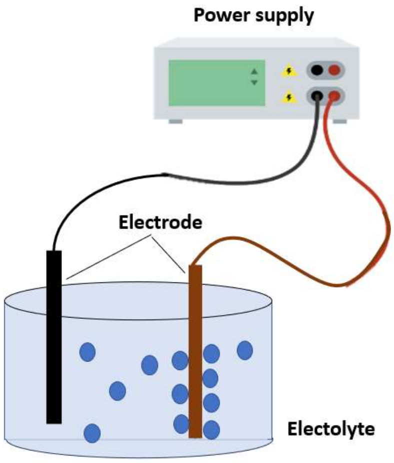

Figure 10: electrophoresis diagram

1.9 Aims

The work developed in this thesis proposes expedite, green and safe strategies to answer to two major health problems: 1) bacterial resistance to the currently used antibiotics and 2) bone-implant rejection due to bacterial infections.

Bacterial resistance can be overcome by synthesizing and redesign new drugs that are capable of by-pass the currently developed mechanisms of bacterial resistance. In view of the objectives to meet environmentally friendly goals, a green synthesis procedure was achieved by mechanochemistry, where no additives were added thus preserving the safety for the pharmaceutical industry. The same pharmaceutical products, tested for their antibacterial properties, are intended to functionalize zinc, a transient metallic implant that represents an improvement over the non-permanent metallic implant already in use. Continuing with the fulfilment of keeping environmentally-friendly goals, the coating technique used, electrophoresis was based on aqueous electrolytes, once more supporting its safety for the environment and human health. The evaluation of the impact of antimicrobial functionalization on zinc degradation is also a goal of this work.

1.10 Physicochemical Characterization Techniques

To attain the proposed goals, several techniques for the physicochemical characterization of the as-synthesized ACFs and functionalized materials were used.
Accurate identification and characterization of the novel compounds are as important as their synthesis. Structural and thermal characterizations are essential for the assessment of the success in developing new ACF forms. This can only be achieved by the combination of different techniques, like powder and single-crystal X-ray diffraction (XRD), differential scanning calorimetry, thermogravimetric analysis, scanning electron microscopy

(SEM), and energy dispersive spectroscopy (EDS). Similarly, the functionalized zinc surface was characterized by XRD, SEM and EDS to guarantee the chemical integrity of the ACF used in the coating formulation. Since this functionalization was made on a biodegradable metallic material, its influence on zinc corrosion behavior was analyzed by electrochemical impedance spectroscopy.

1.10.1 X-ray diffraction

X-rays are a form of electromagnetic radiation that is used for medical imaging tests, cancer treatment, food irradiation, and airport security scanners (*America Society Cancer®*). Most X-rays have wavelengths between 0.01 to 10 nanometers Figure 11, corresponding to frequencies in the range of 30 petahertz to 30 exahertz and energies between 100 eV to 100 keV. This range of wavelength is the ideal to retrieve structural information, recurring to the diffraction phenomena.

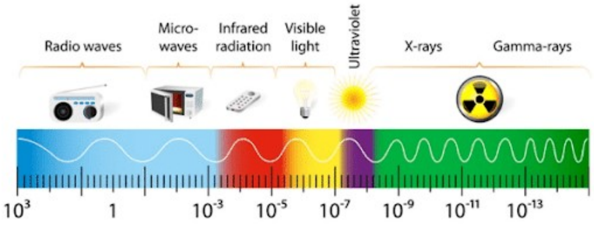

Figure 11: Electromagnetic spectrum

Diffraction is the spreading of waves around obstacles as result of interference, and it is most pronounced when the wavelength of the radiation is comparable to the linear dimensions of the obstacle. This interference can be constructive where the waves are in phase; or destructive when two waves are completely out of phase ((Figure 12).

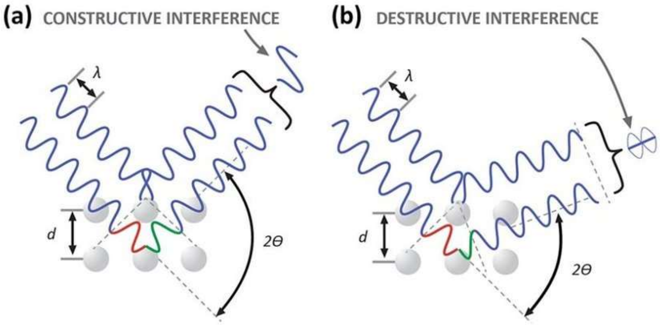

Figure 12:a) constructive interference b) destructive interference(130)

X-ray diffraction (XRD) is a powerful non-destructive structural characterization technique, which allows to synchronize information between chemical and physical properties of materials.

It is known that regarding diffraction “every crystalline substance gives a pattern, the same substance always gives the same pattern and in a mixture of substances each produces it as pattern independently of the others”[134].

X-ray diffraction was discovered in 1912 by Von Laue, Friedich and Knippig, and, in 1913, W.L. Bragg solved the first crystal structure by demonstrating that the angular distance of diffracted radiation can be interpreted considering that the diffracted X-rays behave similarly to what they would if they were reflected by planes passing through points in the crystal lattice. This "reflection" is analogous to that of a mirror for which the angle of incidence of the radiation is equal to reflection angle. Diffracted waves from adjacent planes will be in phase for some angles and the difference in the paths of the two waves is equal to an integer of the wavelength ($n\lambda$). For these conditions, Bragg's Law is proposed (equation 1):

$$n\lambda = 2d \sin\theta \qquad (1)$$

where λ represents the wavelength, *n* an integer, *d* the perpendicular spacing between the planes in the crystal and θ is the complementary angle of incidence of the X radiation beam. Bragg's Law conditions are represented in Figure 13.

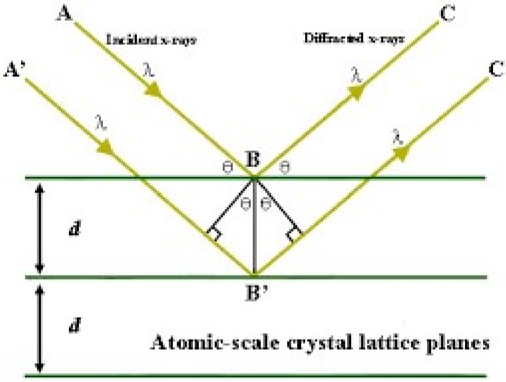

Figure 13: Bragg's Law reflection.(131)

Crystalline materials may be described as function of the crystal lattice, which is defined as a regular periodic arrangement of point in space, being nevertheless a purely mathematical abstraction. The nomenclature refers to the fact that a three-dimensional grid of lines can be used to connect the lattice points. It is important to note that the points of a structure can be connected in several ways to form an infinite number of different network structures. The crystal structure is formed only when the fundamental unit is identically connected to each lattice point and extended along each crystal axis through the repetition of translation.

The basic structural unit is the unit cell that contains one or more molecules, and is defined by three vectors and three angles, as defined in Figure 14. Conventionally, translational vectors are denoted by a, b and c, and the angles by α, β and γ[137].

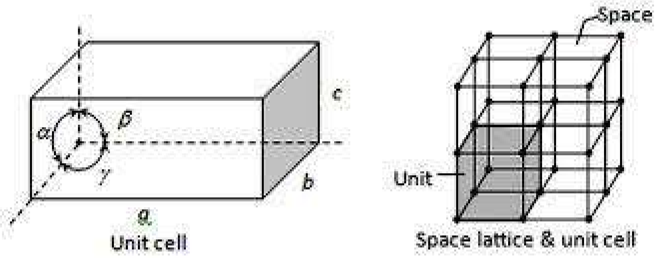

Figure 14: Crystal lattice unit cells(132)

The lattice plane of a given Bravais lattice is a plane (or family of parallel planes) whose intersections with the lattice (or any crystalline structure of that lattice) are periodic and intersect the Bravais lattice; similarly, a lattice plane is any plane containing at least three noncollinear Bravais lattice points. All lattice planes can be described by a set of integers, called Miller indices, and vice versa (all integer Miller indices define lattice planes). Furthermore, there are 14 Bravais lattices that are grouped into 7 crystal systems (Table 3).

Table 3: Characteristic Crystal Systems

Crystalline system	Angles
Cubic	$a = b = c;\ \alpha = \beta = \gamma = 90°$
Monoclinic	$a \neq b \neq c;\ \alpha = \gamma = 90°;\ \beta \neq 90°$
Hexagonal	$a = b \neq c;\ \alpha = \beta = 90°;\ \gamma = 120°$
Orthorhombic	$a \neq b \neq c;\ \alpha = \beta = \gamma = 90°$
Rhombohedral	$a = b = c;\ \alpha = \beta = \gamma\ (\neq 90°)$
Tetragonal	$a = b \neq c;\ \alpha = \beta = \gamma = 90°$
Triclinic	$a \neq b \neq c;\ \alpha \neq \beta \neq \gamma \neq 90°$

Currently, XRD methods are the most reliable to provide more detailed information on the crystal structure, allowing to calculate interatomic distances, bond angles and other relevant characteristics of molecular geometry. The outcome information allows the three-dimensional representation of the crystal's content at the atomic level and the access to most geometric details regarding the crystal structure and supramolecular arrangement.

1.10.1.1 Single Crystal X-Ray diffraction

Single-crystal XRD (SCXRD) involves the assignment of the arrangement of atoms, based on an electron density map generated by diffraction of a pure, regular, and adequately large single crystal. Structural information derived from an XRD study of a single crystal is the most fundamental description of a compound and often facilitates to explain its physicochemical properties. SCXRD is a powerful technique used to determine details of the molecular and crystalline structure of a solid, such as bond lengths, bond angles, intermolecular interactions, etc. The SCXRD experimental setup is represented at Figure 15.

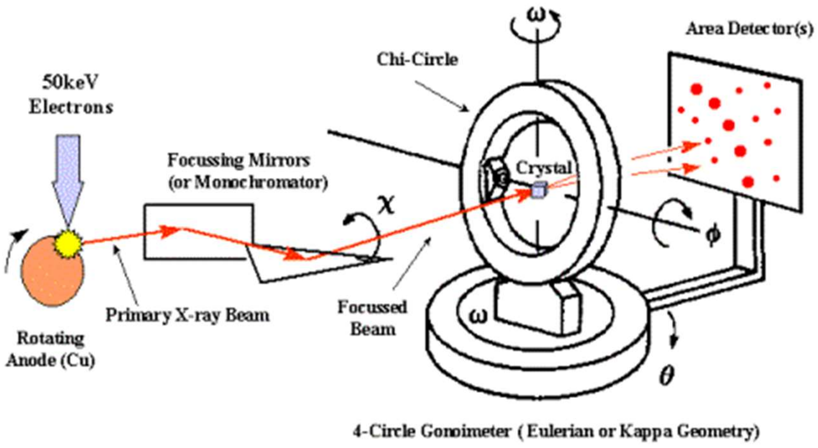

Figure 15: Experimental set-up for Single Crystal X-ray Diffraction (taken from(134))

The three-dimensional results are obtained from diffraction data collected in three dimensions and can be used to computationally simulate the expected two-dimensional powder diffraction pattern of the same material.

1.10.1.2 Powder X-Ray diffraction

Powder X-ray diffraction (PXRD) patterns consist of a series of peaks having varying intensities, detected at various scattering angles (Figure 16). Through the indexing process, the d-spacings computed from the values of the scattering angles are assigned to diffraction from the crystal planes defined by their Miller indices to provide a full crystallographic characterization of the powder sample. Data recorded in the detector is the X-ray intensity (in counts/second, for example). By plotting the intensity against the angle of the incident X-ray, a series of peaks can produce. These diffraction peaks correspond to d-spacing and can be converted using the Bragg equation.

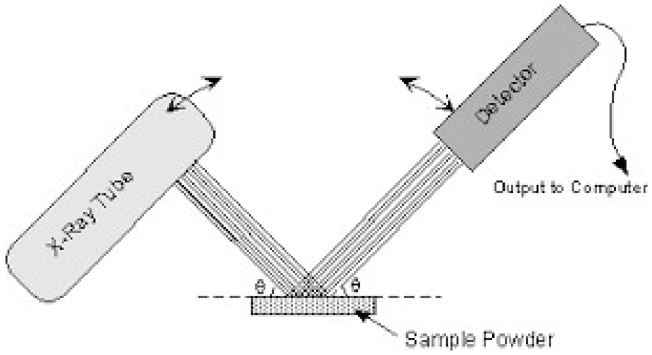

Figure 16: Experimental setup for powder X-ray diffraction (taken from(134))

1.10.2 Thermal analysis

Thermal analysis methods can be appropriately defined as those techniques in which one property of the analyte is measured as a function of an externally applied temperature. In most applications, the effect of a linear increase in the temperature of the sample in the property of interest is recorded on a continuous basis. Thermoanalytical methods are used to monitor endothermic processes (i.e., melting, boiling, sublimation, vaporization, desolvation, solid–solid phase transitions, and chemical degradation) as well as exothermic processes (i.e., crystallization and oxidative decomposition).

1.10.2.1 Differential Scanning Calorimetry (DSC)

In Differential Scanning Calorimetry (DSC), which is the most widely used technique for thermal characterization of pharmaceuticals, the analyte is subjected to a controlled temperature program and the heat flow associated with a thermally induced transition is measured. The basic principle behind this technique is that a change in the baseline of a typical DSC plot (power vs. temperature), corresponds to a thermal event, with a variation in the heat capacity of the system under investigation.

1.10.2.2 Thermogravimetry

Thermogravimetry (TG) or thermogravimetric analysis (TGA) is a technique where one uses a very sensitive balance to continuously determine the weight of the analyte as a function of temperature or time. This simple technique provides valuable information that can be of great assistance in identifying for example solvents, cations or decomposition products.

1.10.3 Scanning Electron Microscopy

Scanning electron microscopy (SEM) uses a focused beam of high-energy electrons to generate a variety of signals at the surface of solid samples. The signals that derive from electron-sample interactions reveal information about the sample including external morphology (texture), chemical composition, and crystalline structure and orientation of the materials making up the sample. In most applications, data are collected over a selected area of the surface, and a 2-D image is generated that displays spatial variations in these properties. Areas ranging from approximately 1 cm to 5 μm in width can be imaged in a scanning mode using conventional SEM techniques (magnification ranging from 20X to approximately 30,000X, spatial resolution of 50 to 100 nm). SEM is also capable of performing analyses of selected point locations on the sample; this approach is especially useful in qualitatively or semi-quantitatively determining of chemical compositions (using EDS - Energy Dispersive Spectroscopy).

Accelerated electrons in an SEM carry significant amounts of kinetic energy, and this energy is dissipated as a variety of signals produced by electron-sample interactions when the incident electrons are decelerated in the solid sample. These signals include secondary electrons (that produce SEM images), backscattered electrons (BSE), diffracted backscattered electrons (EBSD) that are used to determine crystal structures and orientations of minerals), photons (characteristic X-rays that are used for elemental analysis and continuum X-rays), visible light (cathodoluminescence-CL), and heat. Secondary electrons and backscattered electrons are commonly used for imaging samples: secondary electrons are most valuable for showing morphology and topography on samples and backscattered electrons are most valuable for illustrating contrasts in composition in multiphase samples (i.e. for rapid phase discrimination) (135).

1.10.3.1 Energy Dispersive Spectroscopy

Energy Dispersive Spectroscopy (EDS) systems are typically integrated into SEM instruments. These systems include a sensitive X-ray detector, a cooling system, and software to collect and analyze the energy spectrum. A detector is mounted in the sample chamber of the main instrument at the end of a long arm, which is itself cooled by liquid nitrogen. An EDS detector contains a crystal that absorbs the energy of incoming x-rays by ionization, yielding free electrons in the crystal that become conductive and produce an electrical charge bias. The x-ray absorption thus converts the energy of individual X-rays into electrical voltages of proportional size; the electrical pulses correspond to the characteristic x-rays of the element (135).

1.10.4 Electrochemical Impedance Spectroscopy

Electrochemical Impedance Spectroscopy, EIS, is a frequency area measurement made by applying a sinusoidal perturbation, often a voltage, on a system. This analysis is used as a characterization of the electrochemical response of a system where interface behaviors between the electrolyte and surface response (including the coating) that can be inferred from the small perturbations applied.

The impedance at a given frequency is related to the electrochemical processes occurring at timescales of the inverse frequency. While many other electrochemical measurements focus on driving a system far from equilibrium with potential or steps, such as cyclic voltammetry or potentiodynamic curves, EIS uses small perturbations. These small departures from equilibrium are assumed to have a linear response, thus greatly simplifying the frequency analysis; however, linearization of physical models can lead to indistinguishable cases. Essentially, EIS is performed by sweeping through a wide range of frequencies at a single perturbation amplitude. As instrumentation has improved over the last several decades, frequencies ranging from 10^{-2} to 10^{5} Hz are possible, thus allowing for the study of both fast kinetic and mass transport processes.

1.10.4.1 Electrochemical theory and Representation of Complex Impedance Values

Electrical resistance is the ability of a circuit element to resist the flow of electrical current, given by Ohm's law (equation 2) that defines resistance in terms of the ratio between voltage, E, and current, I.

$$R \equiv \frac{E}{I} \tag{2}$$

This methodology operates as an ideal resistor, that has several simplifying properties: a) follows Ohm's Law at all current and voltage levels, b) a resistance value is independent of the frequency, c) alternating current (AC) and voltage signals through a resistor, are in phase with each other. However, was necessary to introduce a more general circuit parameter – impedance, which is a measure of the ability of a circuit to resist the flow of an electrical current, without the simplification provide before.

Measured by applying an AC potential to an electrochemical cell and then measuring the current through the cell, the response to this potential is an AC signal. The current signal can be analyzed as a sum of sinusoidal functions (a Fourier series).

By a small excitation signal for a response pseudo-linear (linear system) the current response to a sinusoidal potential will be a sinusoid at the same frequency but with a phase shift (Figure 17).

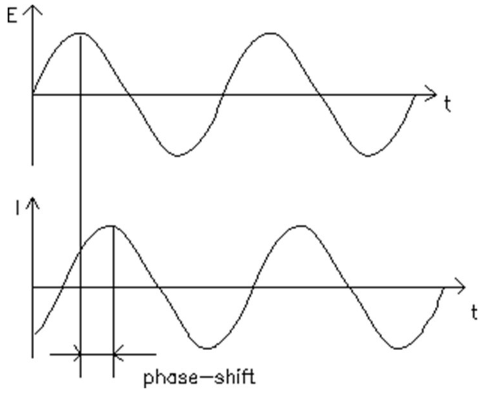

Figure 17: Sinusoidal current response in a linear system

The excitation signal, expressed as a function of time by equation 3, where E is the amplitude of the signal, ω (Hz) is the frequency (ω= 2πf).

$$E_t = E_0 \sin \omega t \tag{3}$$

For a linear system, the response signal (equation 4) is shifted in phase (ϕ) and has a different amplitude than I_0.

$$I_t = E_0 \sin(\omega t + \phi) \tag{4}$$

Similarly, from Ohm's Law it is possible to determine the impedance of a system by using equation ()

$$Z = \frac{E_t}{I_t} = \frac{E_0 \sin(\omega t)}{I_0 \sin(\omega t + \phi)} = Z_0 \frac{\sin(\omega t)}{\sin(\omega t + \phi)} \tag{5}$$

By plotting the applied sinusoidal signal E(t) on the X-axis of a graph, and the sinusoidal response signal I(t) on the Y-axis, the result is an oval - "Lissajous Figure". Analysis of Lissajous Figures on oscilloscope screens was the accepted method of impedance measurement prior to the availability of modern EIS instrumentation. With Euler's relationship, it is possible to express the impedance as a complex function (equation 6).

$$Z(\omega) = \frac{E}{I} = Z_0 exp(j\phi) = Z_0(cos\phi + jsin(\phi)) \tag{6}$$

The expression for Z(ω), which is composed of a real and an imaginary part, is represented by "Nyquist Plot" (Figure 18a). Y-axis is negative and that each point on the Nyquist Plot is the impedance at one frequency, low-frequency data are on the right side of the plot and higher frequencies are on the left.

On the Nyquist Plot, the impedance can be represented as a vector (arrow) of length |Z|. The angle between this vector and the X-axis, commonly called the "phase angle", is f (=arg Z). The impedance is plotted with log frequency on the X-axis and both the absolute values of the impedance ($|Z|=Z_0$) and the phase-shift on the Y-axis, defined by "Bode Plot" (figure 18b), does show frequency information.

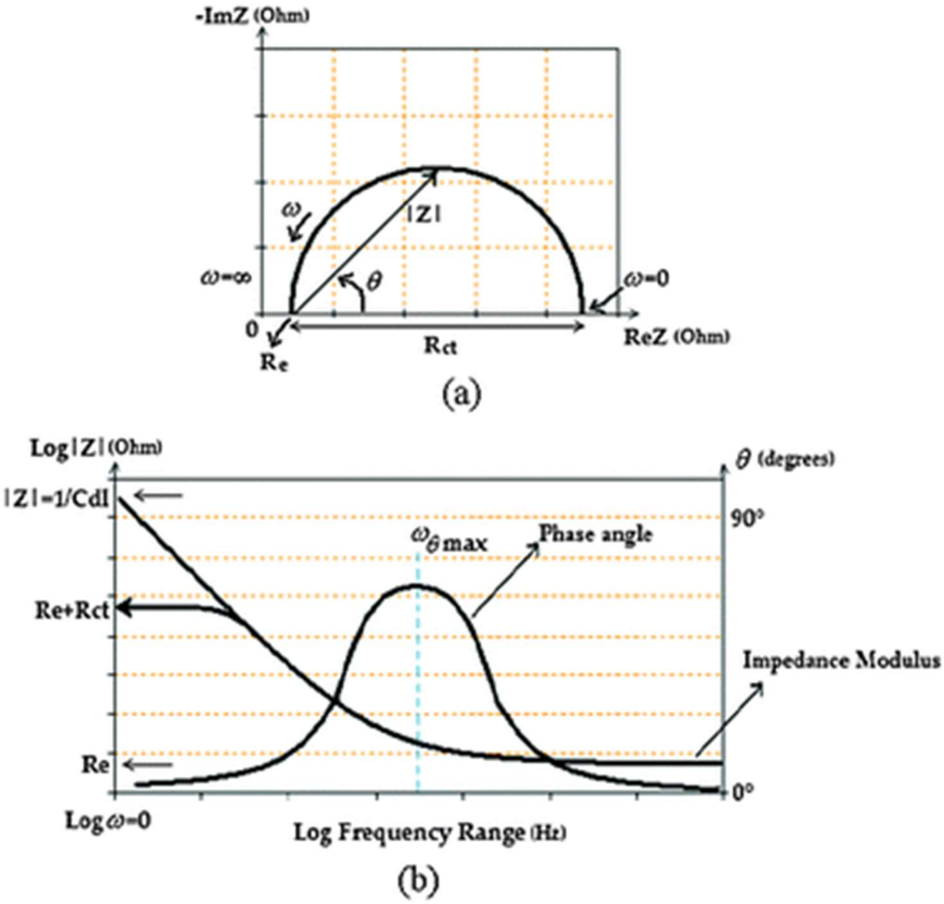

Figure 18: a) Nyquist Plot with Impedance vector; b) Bode Plot (taken from(136)

Electrical circuit theory distinguishes between linear and non-linear systems (circuits), impedance analysis of linear circuits is much easier than analysis of non-linear ones, Figure 19 shows how electrochemical systems can be pseudo-linear. If was analyzed a small enough portion of a cell's current versus voltage curve, a linear system appears (Figure 19) (137).

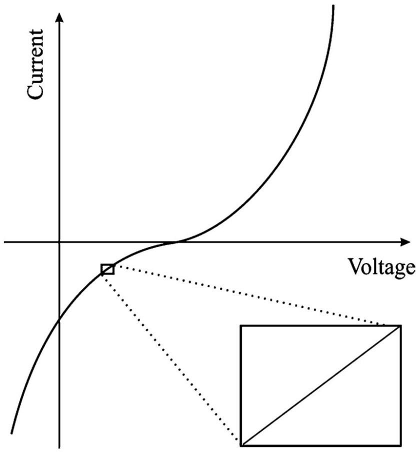

Figure 19: Current versus Voltage Curve Showing Pseudo-Linearity

The system being measured must be at a steady-state throughout the time required to measure the EIS spectrum, in practice a steady state can be difficult to achieve. The cell can change through adsorption of solution impurities, growth of an oxide layer, build-up of reaction products in solution, coating degradation, or temperature changes (138).

1.10.4.2 Electrical Circuit Elements

EIS data are commonly analyzed by fitting with an equivalent electrical circuit model (EEC). Most of the circuit elements in the model are common electrical elements such as resistors, capacitors, and inductors. To be useful, the elements in the model should have a basis in the physical electrochemistry of the system. As an example, many EECs contain a resistor that models the resistance of the solution on the electrochemical cell.

Some knowledge of the impedance of the standard circuit components is therefore quite useful. Table 4 lists the most common circuit elements, the equation for their current versus voltage relationship, and their impedance.

Table 4: Common Electrical Elements

Component	Current Vs. Voltage	Impedance
resistor	E= IR	Z = R
inductor	E = L di/dt	Z = jωL
capacitor	I = C dE/dt	Z = 1/jωC

The impedance of a resistor is independent of the frequency and has no imaginary component, only a real impedance component, the current through a resistor stays in phase with the voltage across the resistor. The impedance of an inductor increases as the frequency increases, inductors have only an imaginary impedance component. The impedance versus frequency behavior of a capacitor is opposite to that of an inductor. A capacitor's impedance decreases as the frequency is raised. Capacitors also have only an imaginary impedance component. The current through a capacitor is phase-shifted 90 degrees with respect to the voltage.

The total impedance of an electrical circuit, at a given frequency, depends on the individual impedance of each element (capacitor and resistor), as an example for a one-time constant, the equivalent circuit is given by Figure 20.

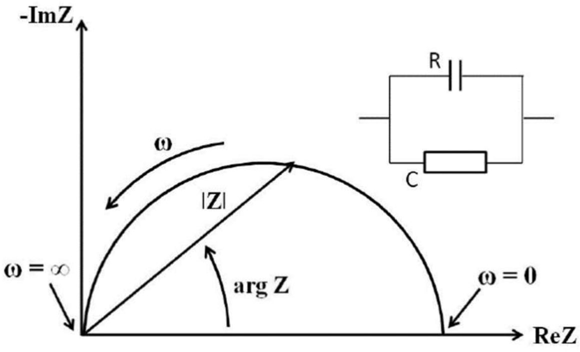

Figure 20: Nyquist Plot with Impedance vector and their equivalent circuit for one time constant

Each association of a capacitor with resistance, when added in series or parallel, corresponds to new time constants, used to describe more complex systems (139).

1.10.5 Solution Simulated Body Fluid (SBF) Protocol

The bone-bonding ability of a material is frequently evaluated by analyzing the capability of apatite to form on the surface using simulated body fluid (SBF), that has an ion concentration nearly to that of human blood plasma(140). SBF was first introduced by *Kokubo* (141)(Table 5), in order to evaluate its changes and reactions on bioactive surfaces of ceramic glasses.

Table 5: Ion concentrations (mM) of SBF and human blood plasma

Ion	**Simulate Body Fluid (141)**	**Blood plasma (140)**
Na^+	142.0	142.0
K^+	5.0	5.0
Mg^{2+}	1.5	1.5
Ca^{2+}	2.5	2.5
Cl^-	148.8	103.0
HCO_3^-	4.2	27.0
HPO_4^{2-}	1.0	1.0
SO_4^{2-}	0.5	0.5

This means that the *in vivo* bone bioactivity of a material can be predicted from the formation of apatite on its surface when immersed in the SBF. Since then, the *in vivo* bone bioactivity of various materials have been assessed by the formation of apatite in SBF.

The preparation of the SBF solution requires two precautions. On the one hand, it is necessary to ensure that all laboratory material is properly cleaned, to avoid contamination and the development of microorganisms in the solution. On the other hand, it is necessary to adjust the pH of the solution to 7.4 after adding all the components, without the precipitation of the salt already in the solution. The SBF solution was prepared on a heating plate and the temperature and pH were monitored during preparation with a thermo and pH probe, respectively. At the end, the pH was stabilized at 7.4 and 37ºC. The amount of reagents used and the order of adding them is described in Table 6.

Table 6: Regents used for preparing SBF (pH 7.40, 1L solution)

Order of adding	**Reagent**	**Amount**
1	$NaCl$	7.996 g
2	$NaHCO_3$	0.350 g
3	KCl	0.224 g
4	$K_2HPO_4 \cdot 3H2O$	0.228 g
5	$MgCl_2 \cdot 6H2O$	0.305 g
6	1M-HCl	5mL + amount to maintain pH (max. 35mL)
7	$CaCl_2$	0.278 g
8	Na_2SO_4	0.071 g
9	$(CH_2OH)_3CNH_2$	6.057 g

B EXPERIMENTAL SECTION

In this chapter, it will be described how the different techniques and procedures were used to develop the research relating to the (i) MOF synthesis, (ii) fabrication of a MOF-based coating on Zn, and (iii) assessment of the in-vitro behavior of the functionalized material.

The methodology used to synthesize the new ACFs, compounds and equipment used will be detailed. After, the technique used to design the ACF coating, materials used, as well as substrate preparation and cleaning procedures will be presented. In both sections, a detailed physicochemical characterization of the ACF and coating respectively were performed. Finally, the degradation behavior of the functionalized zinc was assessed, and the resulting morphological and chemical changes were investigated.

2 Materials and Methods

2.1 Synthesis of the ACFs

The starting materials were purchased and used without further purification. Their specifications are assigned in Table 7.

Table 7: Reagents' specifications

Reagent	Produced	Purity	Physical State
Nalidixic acid	Sigma- Aldrich, Munich, Germany	98%	Solid
Nicotinic acid	Fluka, Buchs, Switzerland	99.5%	Solid
Isonicotinic acid	Sigma- Aldrich, Munich, Germany	99%	Solid
Salicylic acid	Fluka, Buchs, Switzerland	99%	Solid
Calcium hydroxide	Sigma- Aldrich, Munich, Germany	96%	Solid

The structure of the organic ligands is presented in Figure 21.

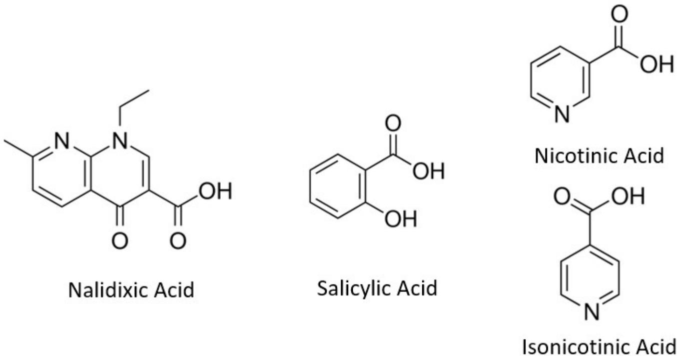

Figure 21: Structure of the organic ligands

All the syntheses were carried out through mechanochemistry. In the first approach, manual grinding was used to assess the viability of the reaction (Figure 22a). A vibrational ball mill was then used to optimize the reaction conditions (Figure 22b). In order to promote the formation of the ACFs, minimum amounts of solvents were used, applying the so-called liquid-assisted grinding (LAG).

Figure 22: a) Different types of grinding jars that can be used for mechanochemistry b) Stainless-steel grinding jars in a Retsch MM400 ball mill

The procedures and description specifications of the conditions tested are shown in Table 7: starting reagents, stoichiometry, solvent quantity and reaction time are described.

Table 8: Experimental conditions of synthesis

ACF	Antibiotic	Co-ligand	Metal	Solvents	Stoichiometry	Time
ACF1	nalidixic acid	salicylic acid	calcium hydroxide	Water 200µl	3:1:2	5 min
ACF2	nalidixic acid	nicotinic acid	calcium hydroxide	Water 200µl	3:1:2	5 min
ACF3	nalidixic acid	isonicotinic acid	calcium hydroxide	Water 200µl	3:1:2	5 min

All the reactions were performed in a Retsch MM400 ball mill operating at a frequency of 29 s^{-1}, using 15 mL stainless steel grinding jars, with 2 stainless steel balls (7 mm diameter).

Single crystals of ACF1 were obtained by recrystallization in methanol and ammonia, by slow evaporation of the solvents, at room temperature. For ACF2, the recrystallization was carried out in MeOH/H2O and MeOH/ N,N-dimetilformamida mixtures. ACF3 single crystals were obtained from a solution reaction in which the starting materials were dissolved in 10 mL of methanol and 1 mL of ammonia and stirred for about 1h at 40^{o}C, and left to crystallize by slow evaporation of the solvents, at room temperature.

All the new structures synthesized were stored at room temperature.

2.2 Coating Formulation

Due to its chemical properties, ACF1 was chosen for the coating formulations studies. This ACF is a compound that results from the coordination of nalidixic acid, used as an antibiotic, and salicylic acid, known as an antimicrobial, to calcium centers, with bone regeneration properties. Moreover, it was shown to be stable after synthesis for several months on shelf conditions.

2.2.1 Substrate Preparation

The specifications of the metallic zinc foil used are listed in Table 9. A previous pretreatment step, necessary to prepare the surface, consisted of polishing with a 360 grain (P600) assisted with water, to level and homogenize the surface; to minimize the formation of oxides at the surface of the substrate, with the same grit was used with ethanol. Finally, the surface was dried with compressed air.

Table 9: Specifications of zinc foil

Zinc Foil Specifications	
Brand	GoodFellow
Purity	99.99%
Temperature	as rolled
Net weight	37.5 g
CAS	7440-66-6

2.2.2 Electrodeposition

To test the best conditions for the electrophoresis of the as-synthesized MOF on zinc, two types of equipment with different current and voltage ranges were used, a Laboratory DC Power Supply Sorensen LH110 (Figure 23a) and a Gamry instruments interface 1010E (Figure 23b). Despite the high voltages used, the stability of operation deposition was performed inside of a Faraday Cage, to reduce any possible noise and avoid possible interferences from external magnetic fields. The noise with an electronic component that exists outside the cage is completely cancelled within that space. All the tests were performed at room temperature.

Figure 23: a) Laboratory DC Power Supply b) Gamry Interface on top couple to a Faraday cage

For the electrophoresis of the new ACF1 on bare zinc, a two-cell system assembly was performed as depicted in Figure 24a). The two-cell system consists of two electrodes with opposite charges (anode, cathode), immerged in an electrolyte. In this system, the anode was a platinum coil, and the cathode was the zinc foil, as schematically represented in Figure 24b.

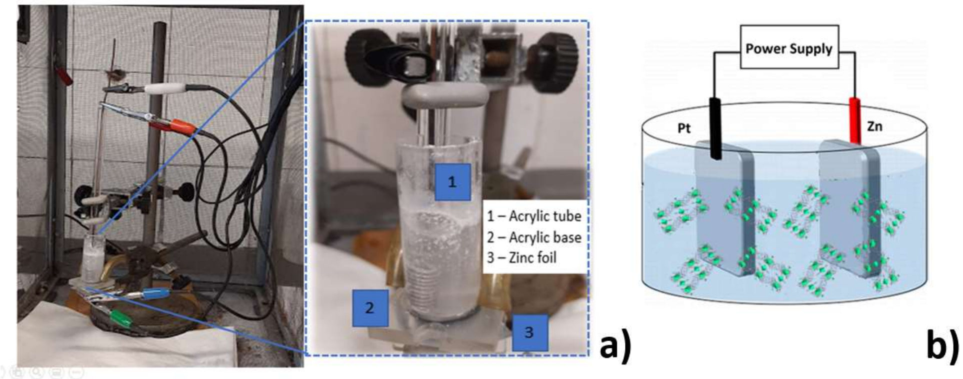

Figure 24: a) Real electrophoresis apparatus, and system cell detailed, b) Scheme of the system

For this experimental step, the assembly of a small volume and a feasible system was achieved with an acrylic cylindrical cell, where the cathode was assembled on the bottom of the cell, with an exposed area of 1.99 cm^2. The electrophoresis tests were performed by applying constant voltages from -12.56V/cm^2 to 25.13V/cm^2, for different periods (60-3600s). The electrolyte was prepared with MilliQ water by adding different concentrations of the ACF1 (1 to 5 mg/mL) to a final volume of 6 mL. Some additives were also added to the electrolyte, namely urea, nicotinamide, and ammonia (Table 10).

Table 10: Reagents for electrolyte preparation

Reagent	Produced	Purity	Physical State
Urea	Sigma- Aldrich, Munich, Germany	99%	Solid
Nicotinamide	Sigma- Aldrich, Munich, Germany	99%	Solid
Ammonia	AnalaR NORMAPUR, Fontenay-sous-Bois, France	25%	Liquid

2.3 In vitro behavior of bare and coated zinc

2.3.1 Preparation of the Simulated Body Fluid

The simulated body fluid (SBF) solution was selected as the medium to study the in vitro degradation behavior and apatite formation of both bare and coated zinc. According to the bibliography(142), and as explained in the introduction chapter, the preparation of the SBF solution occurred at a controlled pH 7.4 and 37°C, using the reagents described in Table 11, and MilliQ water produced in the *Arium®* water system.

Table 11: Reagents used for SBF

Order of adding	Reagent	Produced	Purity	Physical State
1	NaCl	Sigma- Aldrich, Munich, Germany	99.0%	solid
2	$NaHCO_3$	Sigma- Aldrich, Munich, Germany	99.7%	solid
3	KCl	JMGS, Lda, Lisboa, Portugal	99.0%	solid
4	$K_2HPO_4\cdot3H2O$	Merk, Darmstadt, Germany	99.0%	solid
5	$MgCl_2\cdot6H2O$	Merk, Darmstadt, Germany	99.0%	solid
6	1M-HCl	Roth, Karls Ruhe, Germany	98.0%	liquid
7	$CaCl_2\cdot2H_2O$	Merk, Darmstadt, Germany	99.5%	solid
8	Na_2SO_4	Sigma- Aldrich, Munich, Germany	99.0%	solid
9	$(CH_2OH)_3CNH_2$	Sigma- Aldrich, Munich, Germany	99.8%	solid

2.3.2 Degradation behavior

To assess the degradation behavior of bare and coated zinc, electrochemical impedance spectroscopy (EIS) technique was used. These tests were performed by using a Gamry Instruments interface 500+, at 37°C and 50% of humidity. For this setup a three-cell electrode system was used, where the working electrode (WE) was the bare or coated metallic zinc, the counter electrode (CE) was a platinum coil, and the reference electrode (RE) was a saturated calomel electrode (SCE) (Figure 25). The RE electrode is based on the reaction between metallic mercury and mercury (I) chloride. The aqueous phase in contact with mercury and mercury (I) chloride (Hg_2Cl_2, "calomel") is a saturated solution of potassium chloride in water. The electrode is connected by porous medium porcelain to the solution in which the other electrode is immersed. The presence of porous porcelain forms a salt bridge. In a three-electrode cell, the potential is measured between the WE and the RE, while the current measurement is carried out between the WE and the CE. As these measurements are made between different electrode pairs, each measured quantity (potential or current intensity) does not affect the measurement of the other.

Figure 25: System of EIS inside an oven with controlled temperature and humidity

Since EIS is a steady-state technique, to obtain reliable results is important to guarantee the stability of the electrochemical system. Tests of EIS typically start by measuring the open circuit potential (OCP) on day zero for 30min, when the system requires more time to reach a steady-state, whereas in the remaining days of the assays the OCP measurements took 10 min. An electrochemical system is considered stable if the OCP is kept approximately constant over the period of the analysis. To avoid the interference of external electromagnetic noise, essential in these highly sensible tests, all measurements were performed inside an oven that worked as a Faraday Cage. This allowed keeping the operation conditions constant during the seven days of analysis. Temperature and relative humidity (RH) were kept at 37°C to simulate the temperature of the human body, and at 50%, to maintain the % of water on the system, respectively.

The parameters defined for the EIS test, on the Gamry software were: frequency range from 10^{-2} to 10^5 Hz; and 7 points per decade, i. e. seven impedance measurements were made for each variation of the order of magnitude, starting at the highest frequency. The number of points per decade must always be an odd number to avoid resonance with the frequency of the national electricity grid (50 Hz) and its harmonics. Impedance spectra are generally performed with a small amplitude perturbation (typically between 1 – 10 mV). The amplitude of the disturbance was defined as 10 mV for this system. The electrolyte used to assess the degradation behavior of the system was 12mL of SBF solution for an exposed area of the WE of 1.99 cm^2.

2.4 Physicochemical Characterization

2.4.1 Structural, Chemical and Morphological Characterization

Powder X-Ray Diffraction (PXRD): data for ACFs and coated zinc samples were obtained in a D8 Advance Bruker AXS θ–2θ diffractometer (Bruker, Karlsruhe, Germany) equipped with a LYNXEYE-XE detector, using copper radiation source (Cu Kα, λ = 1.5406 Å), operated at 40 kV and 30 mA. Data was collected in the 3–60° 2θ range a step size of 0.02°, and 0.6 s per step.

Single crystal X-Ray Diffraction (SCXRD): Crystals of ACF1, ACF2 and ACF3 suitable for X-ray diffraction studies were mounted on a loop with Fomblin© protective oil. SCXRD data were collected on a Bruker AXS-KAPPA D8QUEST, at 293 K, with graphite-monochromated radiation (Mo Kα, λ=0.71073 Å). The X-ray generator was operated at 50 kV and 30 mA and the X-ray data collection was monitored by the APEX3 program. All data were corrected for Lorentzian polarization and absorption effects using SAINT(142) and SADABS(143) programs. SHELXT(144) was used for structure solution and SHELXL-97(144) was used for full-matrix least-squares refinement on F2. These two programs are included in the package of programs WINGX-Version 2014.1(145). A full-matrix least-squares refinement was used for the non-hydrogen atoms with anisotropic thermal parameters. H_{OH} atoms were added in calculated positions. H_{CH} and H_{OH} atoms were added in calculated positions and refined riding on their respective C and O atoms. Water hydrogen atoms were not modeled. MERCURY 2020.3.0(146) was used for packing diagrams. PLATON(147) was used for hydrogen bond interactions. Refinement details are listed in Table 12.

Table 12: Crystallographic details for ACF1, ACF2 and ACF3

:	ACF1	ACF2	ACF3
Chemical formula	$C_{43}H_{38}N_6O_{20}Ca_2$	$C_{42}H_{37}N_7O_{19}Ca_2$	$C_{42}H_{37}N_7O_{19}Ca_2$
M_r	1037.95	1023.95	1023.95
T / K	298	298	150
Morphology, colour	Block, colourless	Block, colourless	Block, colourless
Crystal size / mm	0.32x0.16x0.02	0.18x0.10x0.04	0.10x0.03x0.02
Crystal system	Triclinic	Triclinic	Triclinic
Space group	*P*-1	*P*-1	*P*-1
a / Å	12.2952(16)	12.2014(8)	12.2221(12)
b / Å	12.6162(15)	12.5343(8)	12.3753(13)
c / Å	16.2844(18)	15.9942(11)	15.8689(18)
α / °	77.517(3)	77.028(3)	78.374(4)
β / °	85.482(3)	85.122(3)	86.490(4)
γ / °	84.262(3)	83.299(3)	83.831(5)
V / Å^3	2449.7(5)	2363.0(3)	2335.4(4)
Z	2	2	2
d / mg.m^{-3}	1.407	1.438	1.456
μ / mm^{-1}	0.316	0.325	0.329
θ range (min -max) / °	2.250 - 26.473	2.691 – 26.535	2.937 – 26.465
Reflections collected/unique	33419/9669	23504/9700	19442/9528
R_{int}	0.1568	0.0643	0.0830
GoF	1.001	1.039	0.994
R_1, wR_2 (> 2σ(I))	0.0932, 0.2320	0.0754, 0.1917	0.0733, 0.1629

Combined *TG-DSC* measurements of the ACF1 were carried out on a SETARAM TG-DTA 92 (Caluire, France) thermobalance under nitrogen flow with a heating rate of 10°C.min^{-1}. The samples weights were in the range of 5-10 mg.

Morphological features of ACF1, and coated zinc samples, before and after the in vitro testes were analyzed by scanning electron microscopy (SEM) using a JEOL-JSM7001F (Tokyo, Japan) or Hitachi S2400 apparatus; for the energy dispersive spectrometer (EDS) analyses the corresponding EDS light elements spectrometers were used, Oxford INCA 250 and Bruker Esprit, respectively. Whenever required, the conductivity of the samples was improved with a thin coating of conductive gold/palladium (Polaron E-5100).

Solubility analyses of the ACF1 were performed by visual inspection when adding 10 mg of ACF1 to 10 mL of different solvents; their properties are presented in Table 13.

Table 13: Solvents' properties used in the solubility tests

Reagent	Produced	Purity	Physical State
Acetone	Honeywell, Riedel-de-Haën, Seelze, Germany	99.5%	Liquid
Ethanol	Carlo Erba, Barcelona, Spain	96.0%	Liquid
Chloroform	Merck, Darmstadt, Germany	99.0%	Liquid

2.4.2 Biological Activity

This biological activity characterization was carried out in full partnership within the project ""ACFs: Antibiotic coordination frameworks as a way to enhance the bioactivity of the drugs" (LISBOA-01-0145-FEDER-030988; PTDC/QUI-OUT/30988/2017) through Dr. Paula Alves, and Prof Patrícia Rijo, to whom I would like to extend my deep gratitude. The operating conditions of the tests are described below.

Gram-negative and Gram-positive bacteria (*Escherichia coli* (ATCC 25922) and *Staphylococcus aureus* (ATCC 25923), respectively) were selected as model organisms for the detection of the minimum inhibitory and bactericidal concentrations (MIC and MBC, respectively) of the synthesized compounds and respective reagents. These values were determined by the microdilution method (148, 149). Briefly, 100 µL of Mueller-Hinton liquid culture medium were added to all the 96-wells of a microplate. Then, solutions of 1mg/ml of the compounds that are going to be tested were prepared. A volume of 100 µL of these solutions was added to the first column and serial dilutions of (1:2) were performed. The final step was the addition of 10 µL of bacterial inoculum to each well. Then, the microplates were incubated for 24 h at 37 °C. After 24 h, the plates were visually analyzed and the lower concentration where no visible bacterial growth could be detected was considered as the MIC. Then, the content of wells without active bacterial growth (within the range of concentrations equal and higher to the MIC) was used as inoculum and spread onto a new sterile Mueller-Hinton solid culture medium. These solid medium plates were incubated at 37 °C for 24 h to allow MBC determination, which is the lowest concentration with no visible bacterial growth.

C RESULTS AND DISCUSSION

3 Design, synthesis and characterization of new Ca-nalidixic acid ACFs

The design of the new ACFs was based on the ability of nalidixic acid to deprotonate the carboxylic acid moiety and coordinate to metal centers like Ca(II) via the carbonyl and carboxylate moieties. Nevertheless, the previous results obtained within the group show that often the final product is a coordination complex that does not give rise to coordination frameworks. Bearing this in mind, it was decided to include secondary ligands into the system to promote the formation of metal-organic frameworks. The choice of the ligands was based on several factors: i) their propensity to coordinate to the Ca(II) centers; ii) their compatibility to be used in pharmaceutical formulations; and iii) if possible, have some type of biological effect. Thus, the coformers chosen were salicylic, nicotinic and isonicotinic acids.

Regarding the synthesis of these compounds, the preferred synthetic technique was mechanochemistry. After optimization of the reaction conditions (stoichiometry of the starting materials, solvent used to promote the reaction, number of balls, reaction time), LAG proved to be effective in obtaining the desired final products, with high purity and high yields.

The characterization of the new products by a combination of different techniques was fundamental to determine their crystal structures, assess relevant properties, and check their stability. The results for the characterization of these compounds will be presented below.

3.1 ACF1

ACF1 results from the LAG reaction between nalidixic and salicylic acids with $Ca(OH)_2$ that led to the complete reaction yielding pure ACF1, with the final bulk product having no traces of any of the starting materials (Figure 25a). Good quality single crystals were grown from the recrystallization process, and therefore crystal structure determination was possible from single-crystal X-ray diffraction data. This information further confirmed the purity of the bulk, by the comparison of the diffraction pattern simulated from the crystal structure with the experimental powder diffraction pattern (Figure 26b).

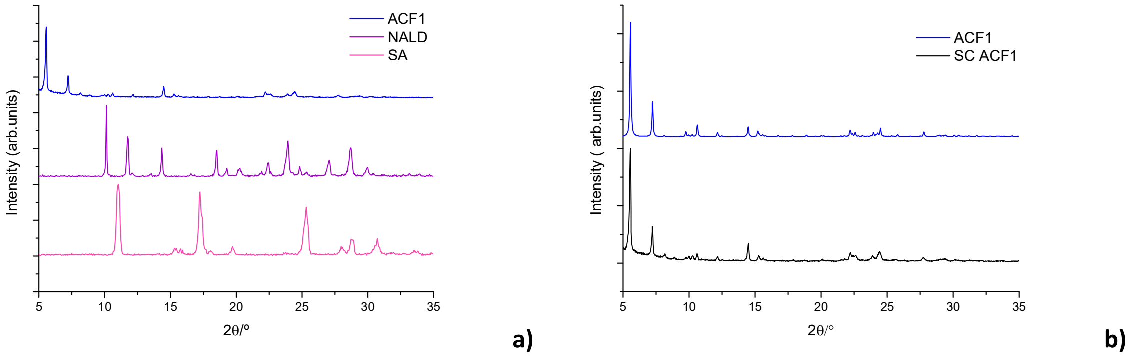

Figure 26: PXRD patterns for a) ACF1 (blue), nalidixic acid (purple), and salicylic acid (pink); b) ACF1 (blue) and pattern from simulated the crystal structure (black)

The reproducibility of the synthetic process was confirmed by PXRD after several the analysis of different batches (Figure 27).

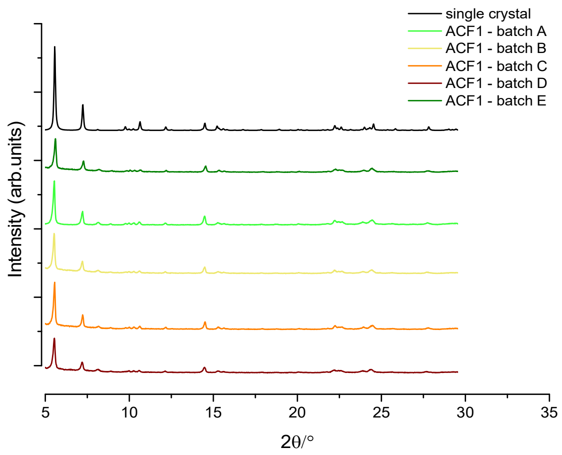

Figure 27: PXRD pattern of ACF1 from different batches compared with the pattern simulated from the crystal structure (black)

Regarding the crystal structure, a brief discussion will be presented, as it is important to understand its main structural features. The asymmetric unit consists of two crystallographically independent Ca(II) metal centers, three nalidixic acid, one salicylic acid, three coordinated water molecules and five hydration water molecules (Figure 28a). In order to coordinate to Ca(II), the carboxylic moieties of nalidixic and salicylic acids are deprotonated. One of the Ca sites coordinates to the three nalidixic acid anions and assumes a square antiprismatic geometry (CN=8), while the other Ca center coordinates to both nalidixic and salicylic acids anions and water molecules displaying an octahedral geometry (CN=6) (Figure 28b).

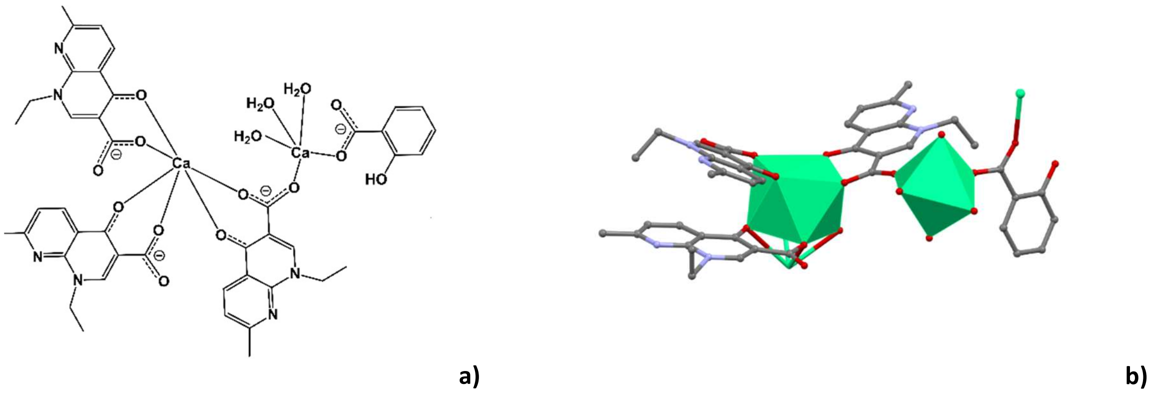

Figure 28: Details on ACF1 crystal structure depicting the: a) details of the coordination to the Ca(II) metal centers; b) coordination Ca(II) geometries. Hydrogen atoms were omitted for clarity

The supramolecular arrangement of ACF1 is characterized by the formation of 1D frameworks, in a view along the *b* axis. Hydration water molecules occupy the space between consecutive 1D frameworks (Figure 29).

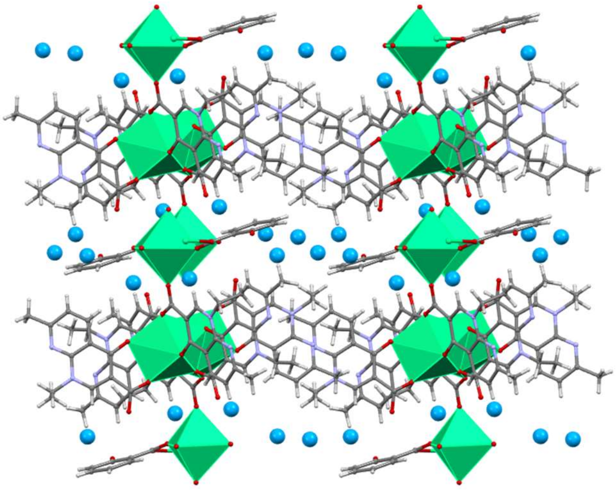

Figure 29: Crystal Packing of ACF1. Hydration water molecules are represented in blue, using space fill style, for clarity

The structure arrangement presents a laminae appearance with length variations between 0.3 to 0.6 µm, with a superior dominance over the minimum length of 0.3 µm (Figure 30a). Distribution of calcium in the structure (Figure 30b) identified an equal distribution of the atoms along all the crystal structure.

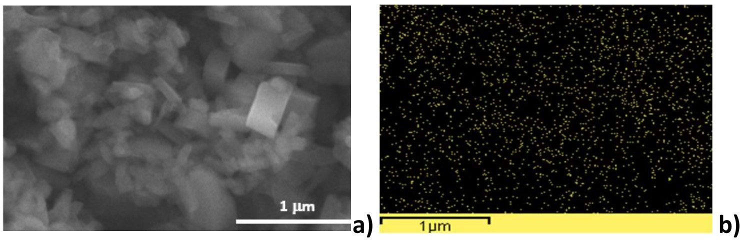

Figure 30: a) Morphological structure of ACF1; b)Atomic distribution of Calcium on ACF1

The atomic percentage attained by EDS of each element is given inTable 13, the elements identified were carbon, oxygen and calcium, all present at the structure of ACF1. Following the crystal structure analyzed on Figure 30a) the percentage of which atom can be estimated. A significant variation on the percentage of carbon was observed, this type of characterization requires the use of a carbon ribbon, an aspect that supports the deviation on values. The elements oxygen and calcium were considered by EDS and the estimated values are in the same range of values.

Table 14: Atomic percentage on ACF1

Element	Carbon	Nitrogen	Oxygen	Calcium
% Atomic by EDS	69.6	n.d.	24.1	6.3
% Atomic estimated	49.0	8.0	30.3	7.6
Deviation	20.6	n.d.	-6.2	-1.3

Analyses of atomic characterization by the ratio between different atoms give a more viable way of comparison of the results. So, ratios between oxygen/carbon and oxygen/calcium were also analyzed, ratio oxygen/calcium was similar to both cases, while oxygen/carbon shown a higher ratio for the same reason that was explained before (Table 14).

Table 15: Atomic ratio on ACF1

Ratio	ACF1 by EDS	ACF1 estimated
Oxygen/carbon	0.3	0.6
Oxygen/calcium	3.8	4.0

ACF1 has shown to be stable over time under shelf conditions, as its crystalline structure is maintained over time (Figure 31).

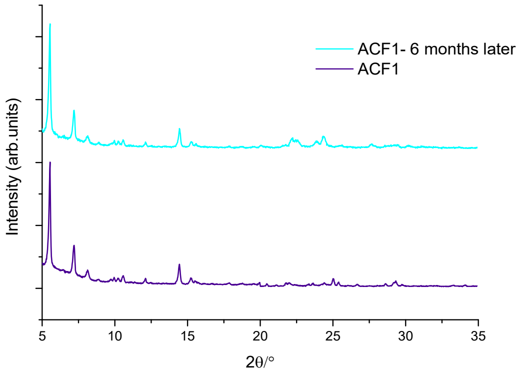

Figure 31: PXRD pattern for ACF1 as-synthesized and ACF1 6 months after synthesis

DSC and TG were obtained for ACF1 to determine its thermal stability. ACF1 is stable until approximately 100°C, the temperature at which the loss water present its structure is detected, corresponding to 11.2% weight loss (theoretical 13.9%) until 120.4°C. After 250°C several decomposition phenomena are detected (Figure 32). From the point of view of the application, this indicates that ACF1 is stable not only at the human body temperature but also in the relevant temperature range for drug storage and transportation.

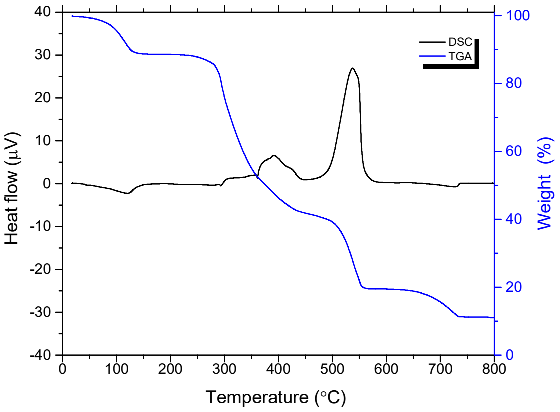

Figure 32: TGA and DSC of ACF1

The antimicrobial activity of the new synthesized ACF1 was tested, as part of a collaboration, against *Escherichia coli* (Gram-negative) and *Staphylococcus aureus* (Gram-positive) bacteria and compared with the activity of the starting materials (Table 15). Results show that the antimicrobial activity is maintained in the new ACF, which is more active *E. coli*, a Gram-negative bacteria, than against *S. aureus*, a Gram-positive bacteria, similarly to nalidixic acid's behavior.

Table 16: Minimal inhibitory concentration (MIC) and minimal bactericidal concentration (MBC) of each reagent and synthesized compound for Escherichia coli *(Gram-negative) and* Staphylococcus aureus *(Gram-positive) bacteria. The compounds' concentration tested ranged from 500 to 0.33 µg/mL*

Compounds	Escherichia coli		Staphylococcus aureus	
	MIC (µg/mL)	MBC (µg/mL)	MIC (µg/mL)	MBC (µg/mL)
Ca(OH)2	125	500	250	500
Nalidixic acid	1.95	>7.81	250	500
Salicylic acid	125	500	250	500
ACF1	1.95	7.81	250	500
Positive control	0.49 (NOR)	Nd	0.98 (VAN)	Nd
Negative control (DMSO)	125	Nd	250	Nd
As a positive control was tested Norfloxacin (NOR) for Gram-negative bacteria and Vancomycin (VAN) was used as positive control for Gram- positive bacteria.				

3.2 ACF2 and ACF3

ACF2 and ACF3 were synthesized by LAG reaction between nalidixic acid, $Ca(OH)_2$ and nicotinic acid or isonicotinic acid, respectively. The final products were obtained as pure phases with high yields (higher than 98%). The powder diffraction patterns were very similar between ACF2 and ACF3, and similar to the one obtained for ACF1, indicating a structural similarity among the three compounds. After recrystallization, it was possible to obtain good quality single crystals for both ACF2 and ACF3 that allowed the structure elucidation and confirmed that the three structures are very similar amongst them (Figure 33).

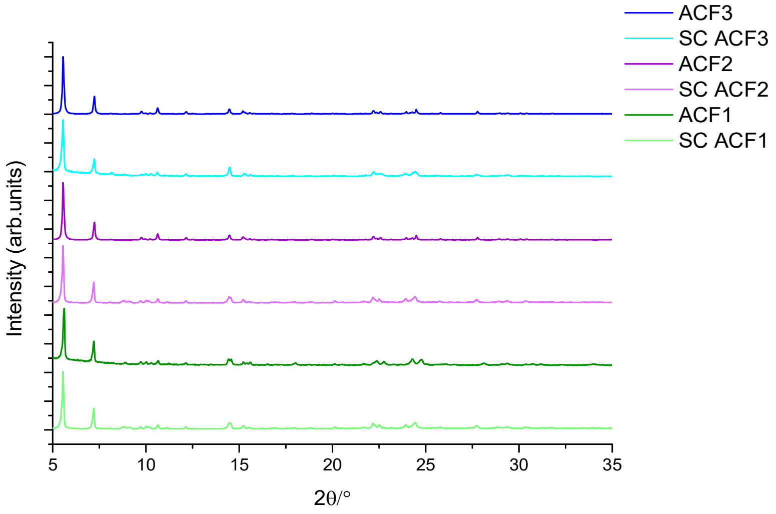

Figure 33: PXRD pattern of ACF3 (dark blue) and pattern from simulated single crystal (light blue), PXRD pattern of ACF2 (dark purple) and pattern from simulated single crystal (light purple), PXRD pattern of ACF1 (dark green) and pattern from simulated single crystal (light green)

Similarly, to what was described for ACF1, also in ACF2 and ACF3, the asymmetric unit consists of two metal centers of calcium, coordinated to three molecules of nalidixic acid via the carboxylate and carbonyl moieties, to a second organic ligand (nicotinic acid for ACF2, and isonicotinic acid for ACF3) via the carboxylate moiety and three water molecules, also enclosing five hydration water molecules (Figure 34). The Ca(II) centers assume antiprismatic (CN=8) and octahedral (CN=6) geometries.

a) **b)**

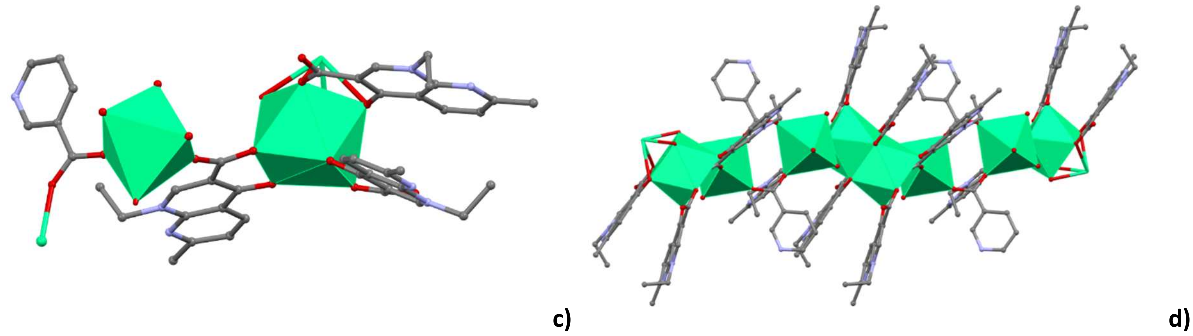

Figure 34: Details on ACF2 and ACF3 crystal structure depicting the: a) details of the coordination to the Ca(II) metal centers in ACF2; b) details of the coordination to the Ca(II) metal centers in ACF3 coordination Ca(II) geometries; c) representation of the geometry around the Ca(II) centers in ACF2; d) representation of the 1D framework formed in ACF2, in a view along the a axis. Hydrogen atoms were omitted in (c) and (d) for clarity

The successful synthesis by mechanochemistry of ACF1, ACF2, ACF3 was easily replicable, according to the operating conditions.

From these three structures, due to the properties of the second ligand, ACF1 was chosen to proceed to the following studies of coating formulation to create a localized drug delivery system.

4 Synthetic Route for the Antimicrobial Coating Formulation

The coating formation was based on the capability that ACF1 has to be deposited on the surface of a metal when an electric charge is applied. This synthetic route, where particles instead of the molecular precursors are used, is called electrophoresis.

4.1 Fine-tuning the coating formulation

As a new and innovative system for coating metals, all variables were unidentified. As such it was necessary to understand how the system reacts to different variables: i) electrolyte composition, ii) applied charge and iii) time of operation.

To select the appropriate electrolyte, solubility analyses of the ACF1 were performed by visual inspection, when adding 10 mg of ACF-1 to 10 mL of a solvent. Visually (data not shown) ACF1 was soluble in chloroform and insoluble in water, acetone and ethanol. For the cases of insoluble solvents and taking into consideration that it will be useful to build a "green" system, water was the selected choice. Having the guarantee that the ACF1 structure was preserved in water, without any risk of modification on its initial structure, this electrolyte was used.

To monitor the changes caused by the applied charge and time variables, different techniques were used to identify the structures/coatings attained at the surface of the substrate.

For the development of this new system, different potentials and deposition times were applied to understand which conditions were leading to the successful deposition of ACF1. By changing the potential from negative to positive values for different periods, it was possible to observe, by visual inspection, that only the positive potential resulted in the deposition of a white coating on the substrate (Figure 35). This evaluation suggests that whatever was being deposited on the zinc surface was negatively charged. As previously shown (Figure 27), ACF1 has a negative charge density, confirming the deposition attained at positive potentials.

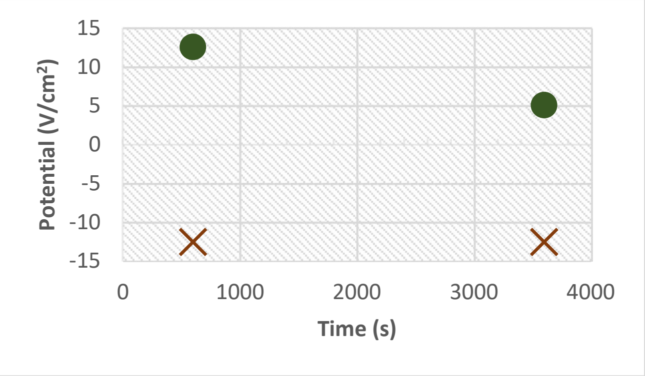

Figure 35: Viability of electrophoresis: green dots represent successful cases, the red cross represents enviably cases [Potential (V/cm^2) vs time(s)].

To confirm that ACF1 was being deposited on the zinc surface and that the electrophoresis was not compromising this MOF PXRD analyses was performed. PXRD confirmed that the stability of ACF1 was kept after the electrophoresis, as the diffractogram of the compound deposited on the surface matches that of the as-synthesized compound (Figure 36). The optimization of the ACF1 coating production, including coating thickness and homogeneity, was explored with positive potentials.

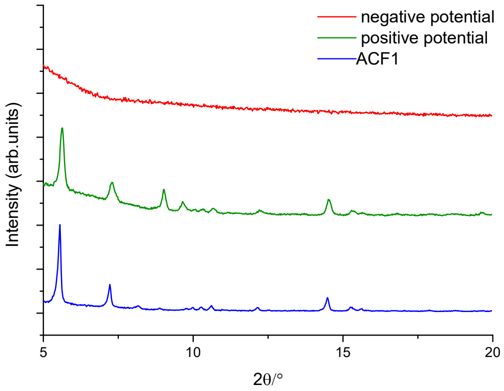

Figure 36: PXRD pattern of the substrate after electrophoresis on negative potential (red), on positive potential (blue) and for ACF1.

To further improve the coating formulation, the concentration of ACF1 was varied. This was quite challenging as the low affinity of the ACF1 to water resulted in the formation of suspensions, limiting the real perception of the effective concentration of ACF1 that was effectively on the electrolyte. Since all the changes in concentration (1 mg/mL, 2 mg/mL e 5mg/mL), in a total volume of 6 mL electrolyte, and time variation (for 3600s and 1200s) at a constant the potential of 2.51V/cm^2 resulted in the deposition of ACF1 on zinc, a more sensitive parameter was required to fine-tune this coating formulation. At this stage, the pH variation observed on the electrolyte upon electrophoresis was chosen. The pH presented variations according to the applied conditions with the most consistent results being attained at 1200s and 3600s. At low concentrations of the ACF, instability was observed for the final pH values, (Table 17). To guarantee reliability of the results, the concentration chosen for further experiments was 5 mg/mL. The hypothesis that proved to be more viable for success was 5mg/mL for periods between 1200s to 3600s (highlighted green on Table 17). In a complex system, where was verified substrate dissolution and can occur rearrangements of ACF, target studies are required to explain these pH changes.

Table 17: conditions of operation of Electrophoresis.

Potential (V/cm^2)	Time (s)	C [ACF1] mg/mL	Electrolyte addition	pH$_{inicial}$	pH$_{final}$
2.51	1200	1	Water	9±1	7±1
2.51	1200	2	Water	9±1	8±1
2.51	1200	5	Water	9±1	11±1
2.51	3600	1	Water	9±1	9±1
2.51	3600	2	Water	9±1	11±1
2.51	3600	5	Water	9±1	11±1

Since the optimization of this coating formulation was an iterative process, the potential values were again different, but at this time by applying small changes. The potentials of 2.51 V/cm^2 and 5.02 V/cm^2 were chosen and applied for 1200s and 3600s. The results at 5.02 V/cm^2 were more consistent, which led to the selection of this as the final potential value to be applied for the fabrication of ACF1 coatings on zinc.

The progress of the system is shown in Figure 37, where the optical images of the coatings attained with the potential and time are presented, as well as the final pH values. In Figure 37, lighter background areas refer to the initial and broader screening of the electrophoresis conditions whereas a darker background refers to a fine-tuning of the selected conditions.

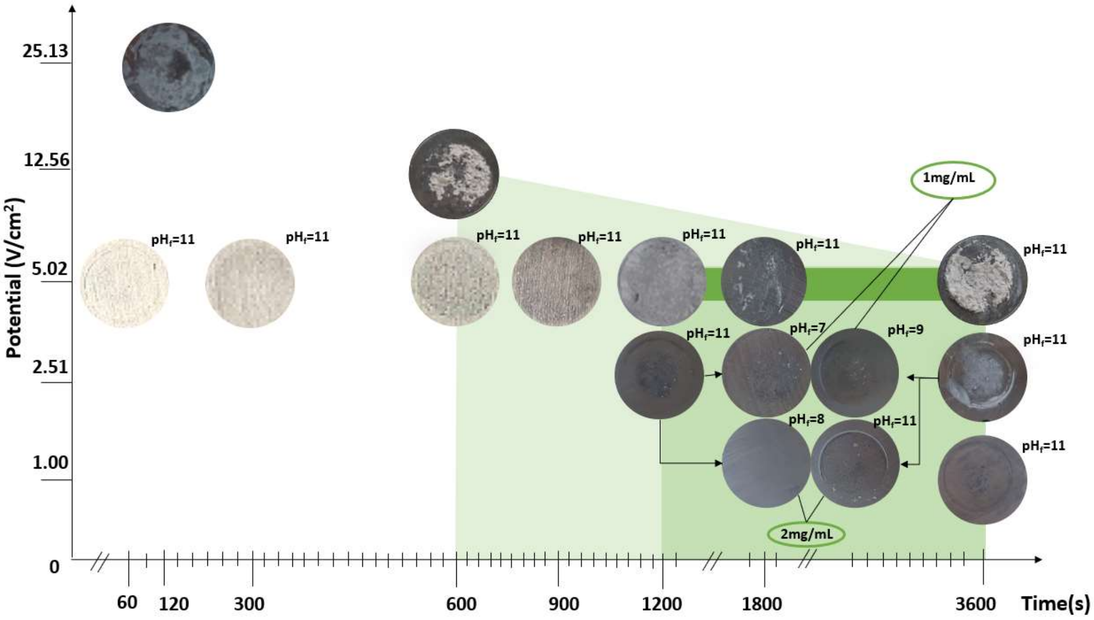

Figure 37: Optical images of the coatings obtained for the different potentials and time used on the electrophoresis procedure; final pH values were added for the relevant cases.

Summarizing, the conditions that led to the successful deposition of ACF1 on zinc by electrophoresis were: i) a concentration of ACF1 of 5 mg/mL, on an electrolyte volume of 6 mL with water, ii) a potential applied of 5.02V/cm^2, and iii) an operation times between 1200 and 3600 seconds.

For an in-depth understanding of the coating formulation, coating attained with 1200 and 3600 seconds were explored.

4.2 In-depth understanding of the coating formulation

To have a deeper insight into the changes occurring in this new and challenging system, the conditions described in Table 18 were analyzed in detail.

Table 18: Parameters used in the synthesis of ZnACF1-1 and ZnACF1-2.

Parameters	ZnACF1-1	ZnACF1-2
Potential (V/cm^2)	5.02	5.02
Concentration ACF1 (mg/mL)	5	5
Time (s)	1200	3600
Electrolyte	water	water

To confirm that a higher potential was not damaging ACF1, the deposits formed were analyzed by XRD. The presence of crystals of ACF1 deposited on the surface of the substrate was confirmed for both cases tested, ZnACF1-1 and ZnACF1-2, therewith at 1200 and 3600 seconds (Figure 38).

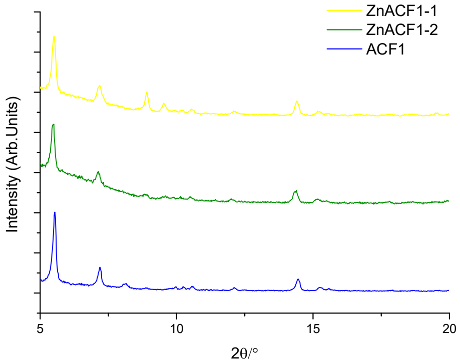

Figure 38: PXRD pattern of the as-synthesized ACF1 (blue), and ZnACF1-1 (green), ZnACF2-2 (yellow) coatings.

The structural analysis of the coatings was also analyzed as well as the substrate surface after deposition. The coatings visual images presented in Figure 39, showed that at the end of the deposition ACF1 was deposited on the substrate.

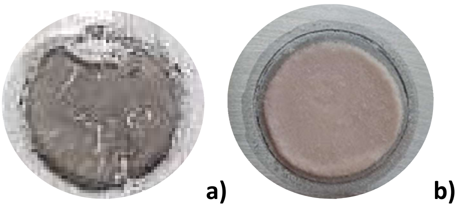

Figure 39: Optical images of the coatings obtained for samples a) ZnACF1-1 and b) ZnACF1-2

A deeper morphological analysis was made by SEM (Figure 40). The substrate surface (without deposition), bare zinc, shows the polishing shafts. In the coated zinc, namely in samples ZnACF1-1 and ZnACF1-2 the presence of a structural form laminae depicted in Figure 40 corroborates the presence of ACF1. Besides ACF1 deposits, were also visible on the surface, as well as several holes caused by Zn degradation. This shows that the ACF1 deposition was made at the expense of Zn dissolution. The main difference between the two coatings is related to the holes formed on the zinc surface, while in ZnACF1-1 there are several and well-defined holes, in ZnACF1-2 the degradation was so extensive that a rough surface (instead of holes) was developed along with the deposition. In both cases, as referred, islands of ACF1 were depicted and additionally in ZnACF1-2 big extensions of ACF1 deposits were also visible on the surface. Interestingly the lamina-like structures of the ACF1 deposits were slightly different, whereas the laminas formed on ZnACF1-1 were smaller when compared with ZnACF1-2, these were larger (insets in Fig. 40).

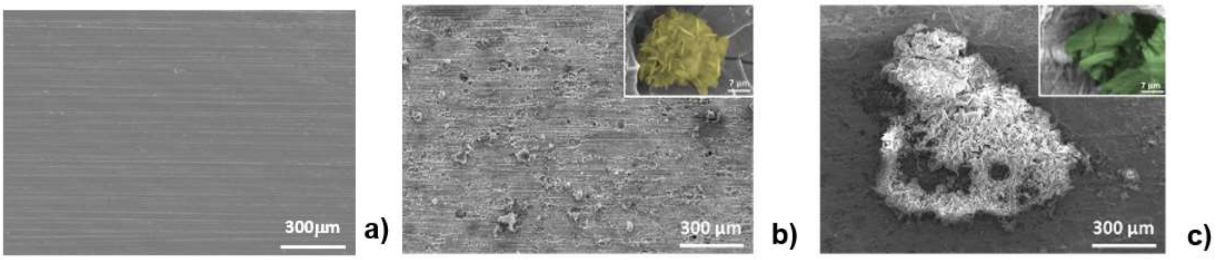

Figure 40: Morphological features of (a) bare zinc and after deposition of ACF1 for 1200s and 3600s, (b) ZnACF1-1 and (c) ZnACF-2, respectively.

To confirm that these laminae-like structures belong to the organic crystalline compound (Figure 40, yellow and green marks) an EDS quantification was made. The elemental compositions, given in table 19, revealed the presence of carbon, zinc, oxygen and calcium. All the organics belong to the ACF1 structure, whereas zinc signal comes from the underneath substrate. When comparing ZnACF1-1 with ACF1-2, the same percentages of carbon and calcium, belonging to ACF1 were detected on the surface. The difference between these two samples was depicted on the Zn:O values, a result that can be related to the analyzed area, i.e., a higher substrate signal was read on the ZnACF1-2 spot than on the ZnACF1-1.

Table 19: Atomic quantification of elements present in coating for samples ZnACF1-1 and ZnACF1-2.

Element	% Atomic SP ZnACF1-1	% Atomic SP ZnACF1-2
Carbon	78.0	78.0
Zinc	12.2	16.7
Oxygen	8.1	3.6
Calcium	1.7	1.7

A comparison between the ratios of ZnACF1 samples (Table 19) with the ones for the as-synthesized ACF1 (Table 15), showed that the ratios of oxygen to calcium were slightly increased on the ZnACF1-1 sample and decreased on the ZnACF1-2 sample. This is a complex system that despite having the same structural packing, can have suffered some chemical modification. Due to the high alkalinization of the medium upon the deposition, the possible hydrolysis of the peripheric carboxylic groups can be hypothesized (Figure 40a), thus decreasing the O content on the material's surface of the sample deposited for a longer period (ZnACF1-2).

Table 20: Ratio of atomic elements carbon/oxygen and carbon/oxygen for cases ZnACF1-1 and ZnACF1-2

Ratio	ZnACF1-1	ZnACF1-2
Oxygen/calcium	4.8	2.1

Despite the successful deposition of ACF1 on zinc, the presence of “holes” (Figure 40) on ZnACF1-1 and ZnACF1-2 were perceptible on the surface. These are a consequence of the imposed potential. By the fact that ACF1 has a negative net charge, its deposition could only be guarantee by imposing a positive voltage, thus using zinc as a sacrificial anode. This strategy caused zinc dissolution, as evidenced by the anodic reaction given by equation 7.

$$Zn(s) \rightarrow Zn^{2+}(aq) + 2e^{-} \tag{7}$$

These holes can bring drawbacks in terms of the degradation rate and mechanical properties. In an attempt to eliminate this unwanted effect, a modification to the original system was made, by applying a cathodic potential on WE, as suggested in previous studies(118). In an attempt to change the global net charge of the ACF1 from negative to positive in the electrolyte, different compounds were dissolved in water. Ideally, a new system formed by ACF1+new compound would result in a positive net charge, thus avoiding zinc dissolution.

4.3 A new system for the coating formulation

These tests were performed by using an electrolyte solution saturated in urea (ZnACF1-3) or niacinamide (ZnACF1-4) with the same but opposite potential -5.02V /cm^2, for 3600 seconds. These additives resulted in the same electrolyte appearance, i.e., a white solution.

After electrophoresis, the sample ZnACF1-3 showed a visual appearance (Figure 41) which did not reveal any modification on the surface of the substrate, clearly revealing the inefficiency of this strategy. The electrolyte appeared yellowish (instead of a white solution) suggesting that a modification on the structure of ACF1 occurred, most probably as a result of ACF1 disintegration. A final pH value of 12, higher than the typically obtained when ACF1 is electrodeposited (Figure 37, pH=11), further corroborates the inadequacy of this strategy. In the case of ZnACF1-4 an altered surface of the substrate was observed (Figure 41), this morphology was completely different in comparison with results shown before(figure 39) This was the morphology before dry (as previously shown in Figure 36). Contrary to ZnACF1-1 or-2, the ZnACF1-4 presented a dark residue on the zinc surface, and the electrolyte an orange coloration; no change in the final pH of the electrolyte was depicted upon electrodeposition, as a final value of 7 was measured.

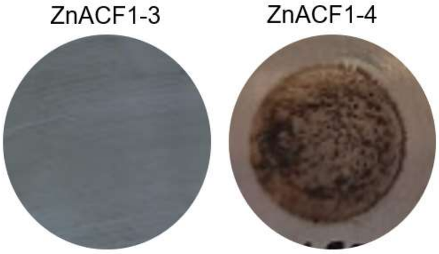

Figure 41: Optical image of the substrate after electrophoresis for cases ZnACF1- 3, and ZnACF1-4.

Even though, physicochemical characterization of ZnACF1-4 was performed. As observed in Figure 42, the type of structures present on the surface with cubic and sphere-like morphologies, have no morphologic similarities to the structure of ACF1 prior (Figure 29a) or after electrophoresis (Figure 40). By the EDS characterization, the presence of all expected elements was identified (Figure 42). The high Ca content, compared with the low C content (Table 19) further evidence that ACF1 structure was compromised, where the Ca released from its structure was precipitated on zinc surface in the form of a different compound (e.g., calcium carbonates).

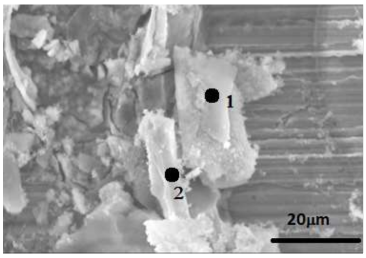

Element	% Atomic SP ZnACF1-4 Point 1	% Atomic SP ZnACF1-4 Point 2
Oxygen	60.9	52.6
Carbon	25.2	25.4
Calcium	7.5	20.9
Zinc	6.4	1.1

Figure 42: Morphology of ZnACF1-4 and the EDS for the same sample

Upon the failure of inverting zinc role from a sacrificial anode to a cathode for the electrophoresis deposition, the real impact of having an ACF1 coating on zinc at the expense of its dissolution was assessed by degradation studies on ZnACF1-1 and ZnACF1-2 using mimicked physiological conditions.

4.4 Degradation behavior

As zinc is well-acknowledged as a bioresorbable material (112, 119), any surface modification can result in an altered degradation behavior. To evaluate these changes, electrochemical and physicochemical analyses were performed under biomimetic conditions. Progressing with the study of the electrochemical behavior of bare zinc and coated zinc, the evolution of the OCP during the immersion, in SBF at 37ºC was registered. This parameter, analyzed for a period of 10 min before impedance spectroscopy, revealed that in the first days there was a variation in the OCP of bare Zn that stabilized after 1 day of immersion (Figure 43); for the ZnACF1-1, such stabilization was achieved as well after the first day, whereas for ZnACF1-2, such a stabilization was not visible for the period of the analysis.

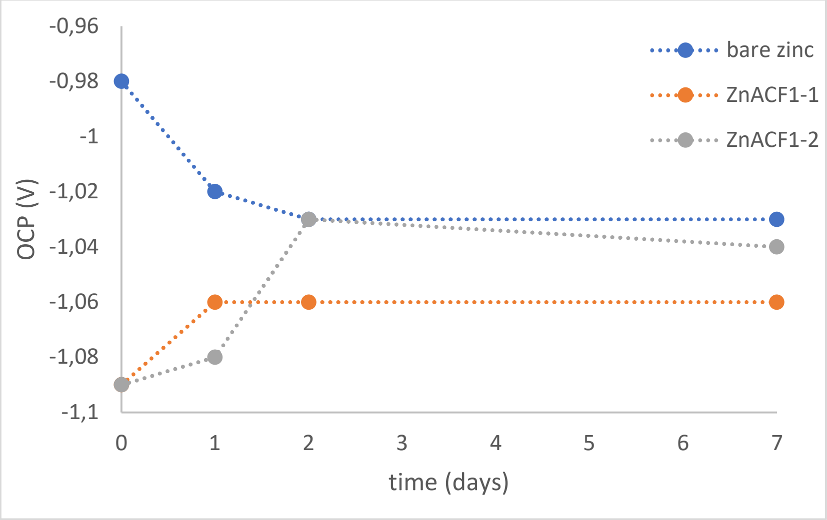

Figure 43: Evolution of OCP of samples: Bare Zinc, ZnACF1-1 and ZnACF1-2, immersed on SBF for 7 days.

Interestingly, for bare zinc the OCP decreased after 6 days of immersion, whereas for the coated samples the was OCP increased, revealing that distinct evolutions were achieved for the bare and coated zinc samples. To have a deeper insight into these changes, EIS measurements were performed. The EIS results, for the samples immersed in SBF at 37°C are presented in Figure 44.

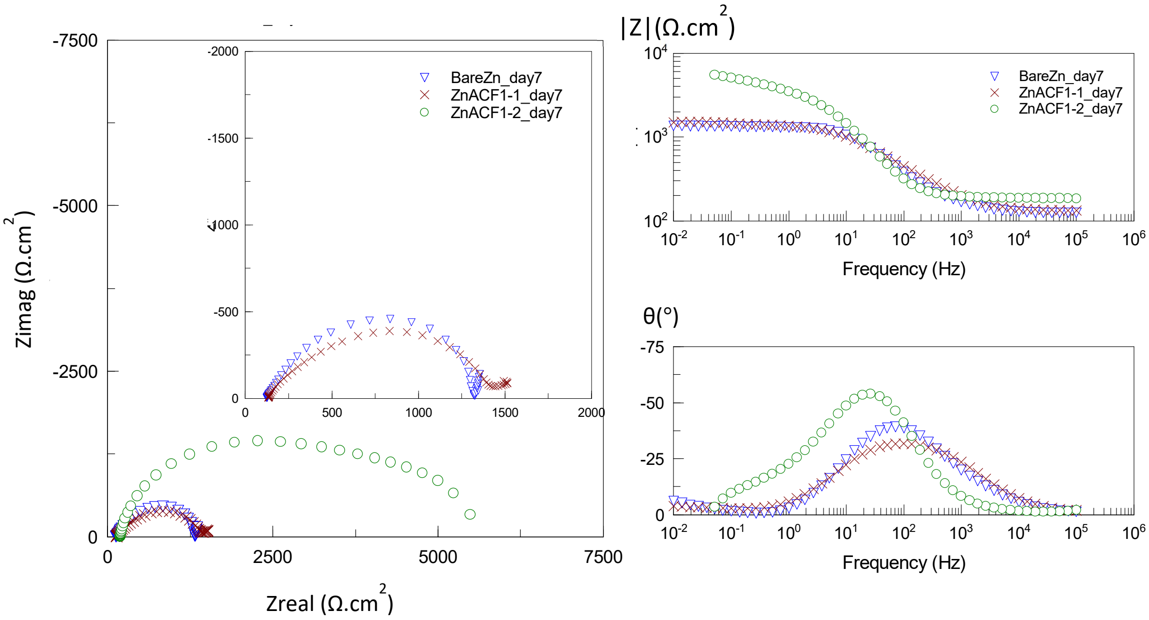

Figure 44:Electrochemical impedance spectroscopy data; Nyquist (left) and Bode plots (right) for Bare Zn, ZnACF1-1 and ZnACF1-2 after 7 days of immersion in SBF at 37ºC

The Nyquist plots showed that both bare Zn and ZnACF1-1 have similar behaviors, with the semi-circles suggesting similar corrosion resistance behaviors; a small slop tending to 45° suggests that active corrosion may be occurring through pitting, which agrees with the holes depicted on this surface (Figure 40). The plot for the ZnACF1-2, with a large semi-circle, indicates a higher corrosion resistance, when compared with bare Zn or ZnACF1-1.

The value of |Z| at lower frequencies shows that ZnACF1-2 has the highest corrosion resistance, whereas both bare Zn and ZnACF1-1 have similar corrosion resistances. These results suggest that, despite the holes formed on ZnACF1-2, the corrosion onset resulted in a more protective surface than in the case of both bare zinc and znACF1-1. This means that upon corroding, the protective effect of the ACF1-2 coating super passed the detrimental effect of the hole formed on the sample surface coating (which due to the extension of Zn dissolution resulted in a rough surface, as explained above, Figure 40). When comparing the phase angle plots, there is clear evidence that the time constant appearing in the middle frequency range, referring to the resulting corrosion products formed upon immersion, are quite distinct. Both in bare zinc and ZnACF1-1, despite the similar protectiveness, the nature of the resulting products is different. The most protective corrosion products, achieved on the ZnACF1-2 sample, are visible by the highest phase angle in the middle-frequency range.

To further disclose the differences in the degradation behaviors observed for Zn, ZnACF1-1 and ZnACF1-2, a detailed physicochemical analysis of the degradation products was performed (Figure 45). Globally, it was possible to conclude that the sample of bare zinc is the one with the smallest area showing corrosion products, compared to the substrates that were previously coated with ACF1. Between samples ZnACF1-1 and ZnACF1-2, the difference in the degradation activity was enormous, the sample that was coated for the longest time resulted in the formation of more corrosion products (ZnACF1-2), which were responsible for the increased protection detected by EIS. It should be noted that, on the coated samples, the presence of ACF1 was not identified morphologically, assuming that has been degraded. Future studies to analyze the release rate and form of degradation of the compound are required. It is noteworthy that the elements present on ACF1 (carbon, oxygen and calcium) promoted the formation of degradation products that can be favorable to the system, in the sense that these can improve the biocompatibility of the designed materials. A deep and complete analysis of the structures obtained should be carried out for an interpretation of the chemical products of corrosion and biocompatibility evaluation.

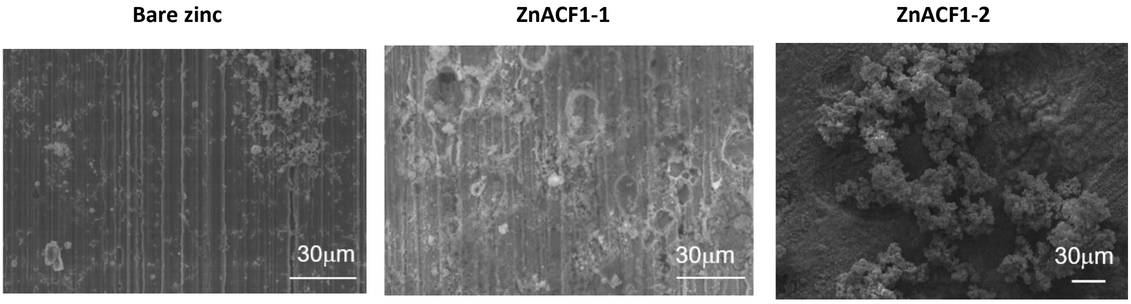

Figure 45: Analysis of the corroded surfaces of bare zinc, ZnACF1-1 and ZnACF1-2 upon immersion in SBF for 7 days at 37°C.

By working with a simulation of plasma, such as SBF, which is rich in physiologically relevant ions, is possible to predict the combination of ions with the released zinc and ACF1 through the chemical elements' analysis on the corroded surface. From the corrosion products reported in other studies (113, 116,118), where zinc behavior was analyzed, new structures were identified, in which elements such as oxygen, carbon, calcium, phosphorus, chlorine and zinc were identified.

On first analysis, zinc oxidation can occur, and is given by equation (8):

$$Zn \rightarrow Zn^{2+} + 2e^{-} \tag{8}$$

The reduction of zinc occurs by producing a precipitate of zinc hydroxide, [$Zn(OH)_2$], equation (9). By the dehydration of zinc, hydroxide is possible to form *zincite*, ZnO, form a typical galvanic couple with Zn which promote an acceleration of corrosion.

$$Zn^{2+} + 2OH^{-} \rightarrow Zn(OH)_2 \tag{9}$$

In presence of carbon dioxide, *zinc hydroxide* can be converted in a new structure *hydrozincite* [$Zn_5(OH)_6(CO_3)_2$], equation 10:

$$5\,Zn(OH)_2 + 2\,CO_2 \rightarrow Zn_5(OH)_6(CO_3)_2 + 2H_2O \tag{10}$$

The presence of zinc hydroxide and zinc oxide in contact with chloride ions promotes the formation of s*imonkolleite* [$Zn_5\,(OH)_8\,(Cl_2)\cdot H_2O$], equations 11 and 12:

$$4\,Zn(OH)_2 + ZnCl_2 + H_2O \rightarrow Zn_5(OH)_8Cl_2 \cdot H_2O \tag{11}$$

$$4\,ZnO + ZnCl_2 + 5\,H_2O \rightarrow Zn_5(OH)_8Cl_2 \cdot H_2O \tag{12}$$

For the presence of zinc oxide simultaneously dissolution of carbon dioxide can occur a new form of precipitate $ZnCO_3$ (*smithsonite*), equation 13:

$$ZnO + HCO_3^{-} \rightarrow ZnCO_3 + OH^{-} \tag{13}$$

Compounds derived from the presence of phosphates in solution have also been reported, *hopeite* [$Zn_3(PO_4)_2$] and *skorpionite* [$Ca_3Zn_2(PO_4)_2CO_3(OH)_2$].

Without any relationship with existing zinc, but with high importance due to the constitution of ACF1 were formed calcium phosphates, *hydroxyapatite*, $Ca_{10}(PO_4)_6(OH)_2$ (equation 14). This is a structure widely studied as a coating to improve the biocompatibility of biomaterials (150-153).

$$2\,CaHPO_4 + 2\,Ca_4\,(PO_4)_2O \rightarrow Ca_{10}\,(PO_4)_6(OH)_2 \tag{14}$$

By the presence of certain chemical elements, was possible to predict the existence of some of these corrosion products on ZnACF1-1 and ZnACF1-2 surfaces. Their elemental relationship is shown in Table 21.

Table 21:Corrosion product and their chemical element composition

Element	**Corrosion product**
Oxygen	*Zincite, hydrozincite, simonkolleite, skorpionite, hydroxyapatite,* smithsonite
Carbon	*Hydrozincite, skorpionite*, *smithsonite*
Calcium	*Hydroxyapatite*
Zinc	*Zincite, hydrozincite, simonkolleite, skorpionite, smithsonite, hopeite*
Phosphorous	*Hydroxyapatite, skorpionite, hopeite*
Chlorine	*Simonkolleite*

Analyzed by EDS, the chemical element composition was identified in each surface region, according to the distinct morphological variations revealed. Following the different morphologies, on bare zinc after seven days of immersion (Figure 46), three morphologically distinct zones were identified: point 1 the precipitated compounds have an elongated geometric shape, that together with C and O contents can suggest the precipitation of carbonates as *hydrozincite, skorpionite, hopeite;* at zone 2 few corrosion products were detected, where Zn predominates, and at point 3 spherical-like structure were and together with higher P contents can be associated to zinc phosphates and/or calcium phosphates like *skorpionite, hydroxyapatite, hopeite;* the presence of *zincite* can be also considered.

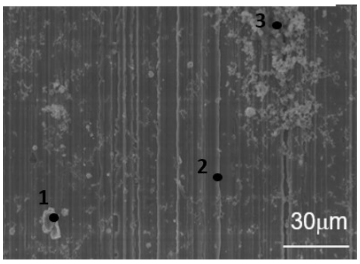

Element	% Atomic SP ZnBare_day7		
	Point 1	**Point 2**	**Point 3**
Oxygen	10.6	11.6	43.8
Carbon	10.8	33.8	n.d.
Calcium	0.7	n.d.	1.2
Zinc	75.2	54.0	42.9
Phosphorous	2.7	0.5	10.4

Figure 46: Physicochemical analysis of the corrosion products formed on zinc bare, and corresponding atomic quantification by EDS

On sample ZnACF1-1 after seven days of immersion (Figure 47) a larger area with corrosion compounds can be depicted. Morphologically was observed different zones, there is a significant difference in brightness intensity between 1 and 2, which the contrast in the image is due to the absorption of electrons by the material, on that case suggests the existence of distinct corrosion compounds. On full analysis was revealed the existence of a new element, chlorine, without loss of any of the elements described before, which suggest that an additional corrosion product was formed, *Simonkolleite.*

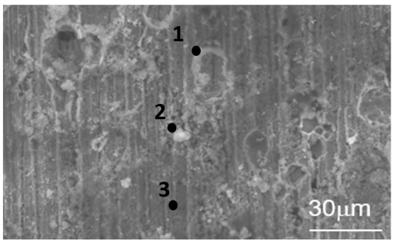

Element	% Atomic SP ZnACF1-1_day7		
	Point 1	**Point 2**	**Point 3**
Oxygen	20.2	53.1	25.9
Carbon	16.9	13.3	14.1
Calcium	4.1	3.4	1.6
Zinc	48.2	22.3	53.1
Phosphorous	9.5	7.4	5.1
Chlorine	1.1	0.5	n.d.

Figure 47: Physicochemical analysis of the corrosion products formed on ZnACF1-1, and corresponding atomic quantification by EDS

As described in ZnACF1-1, the elements identified were the same. The major difference occurred in the layer of products deposited on this sample. From the bare zinc and ZnACF1-1, ZnACF1-2 is by far the sample with more corrosion products (Figure 48). So, corrosion products such as *hydrozincite, skorpionite, hopeite, zincite*, *skorpionite, hydroxyapatite, hopeite* and *simonkolleite* are expected to be found in this layer.

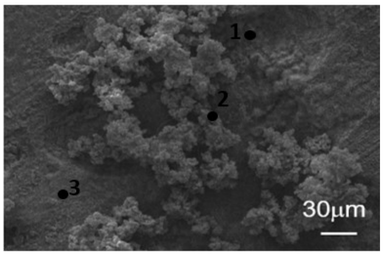

Element	% Atomic SP ZnACF1-2_day7		
	Point 1	Point 2	Point 3
Oxygen	49.8	56.6	24.2
Carbon	9.1	18.1	16.5
Calcium	7.8	3.9	1.9
Zinc	23.1	18.3	50.2
Phosphorous	10.3	3.2	5.4
Chlorine	n.d.	n.d.	1.8

Figure 48: Physicochemical analysis of the corrosion products formed on ZnACF1-2, and corresponding atomic quantification by EDS

Upon an overall comparison of the corrosion products formed on ZnACF1-1 (Figure 47) and ZnACF1-2 (Figure 48), there is a notable increase in Ca content in ZnACF1-2. This, expected to form hydroxyapatite can endow ZnACF1-2 with increased biocompatibility.

In an attempt to identify this important inorganic compound, the corroded substrates were analyzed by XRD. For sample ZnACF1-1 no signs of crystalline corrosion products were recorded. Whatsoever, a peak was successfully obtained for the corroded ZnACF1-2 sample for a theta value of approximately 11°, a peak that is regularly identified in the literature for the presence of hydroxyapatite (154-156).

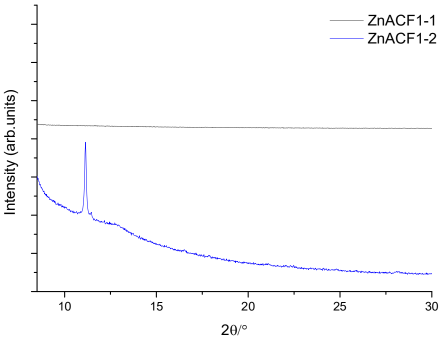

Figure 49: PXRD pattern of substrate after immersion for sample ZnACF1-1 (black) and ZnACF1-2 (blue)

The high Ca content (Figure 48) and XRD analysis (Figure 49) are strong indications for the formation of calcium phosphates, a compound that has a major interest in this study, as it is shown to be important on the success of bone implants. By improving the cytocompatibility with human bone cells, is responsible to promote osteoconductive and promote biosorption properties. The increased capability of reabsorption of molecules responsible for the recovery of bone may therefore improve the desirable properties of the biomaterial presented herein.

D CONCLUSIONS

New antibiotic coordination frameworks represent a possible alternative with many advantages to the pharmaceutical industry. Three new ACF structures (ACF1, ACF2 and ACF3) were described herein, corresponding to the coordination of nalidixic acid and a second ligand (salicylic, nicotinic and isonicotinic acids, respectively) to Ca(II). Mechanochemistry, the synthetic method used, is a very important aspect of this work, as nowadays both academia and industry are requested to explore sustainable methods, as the one presented, for new drugs production.

The structure of the new compounds was fully elucidated by the X-ray diffraction techniques, revealing that, despite the different second ligands used, the final ACF structures were very similar and characterized as 1D frameworks. Due to the bioactive interest of ACF1 - anti-inflammatory and antibacterial activities, the stability studies performed, proved its stability for shelf-lives of at least 6 months, and temperatures up to approximately 100ºC. These are important aspects for pharmaceutical industries, as storage and transportation represent significant costs on new drugs commercialization.

As part of a collaboration, it was possible to confirm the antimicrobial activity of ACF1 against *E. coli*, a Gram-negative bacteria, and *S. aureus*, a Gram-positive bacteria. This new and reinforced structure, when compared with nalidixic acid alone, presents new solutions for bioactive and antibacterial coatings design.

The deposition of the new ACF1 on zinc was successfully achieved by green and safe electrophoretic procedures. The deposition of ACF1, made at the expense of zinc dissolution, delivered materials with a higher degradation activity. This activity together with ACF1 dissolution led to the formation of highly biocompatible corrosion layers where hydroxyapatite, an important bone analogue, was formed.

The innovative system presented in this thesis, for the design of robust bioactive and antibacterial ACFs for zinc functionalization, opened the door for a new line of research on local drug delivery systems.

E FUTURE PERSPECTIVES

Due to the success achieved on the mechanochemical synthesis of the new metal-organic drug structures, the studies on the antimicrobial activity should be extended, namely towards antibiotic-resistant bacteria, as MRSA and fungi, like pathogenic *Candida* spp. Moreover, by changing the second ligand, new chemical and biological properties can be achieved to expand these ACFs to different areas of treatment, namely in cardiovascular diseases.

The approach presented herein, regarding surface engineering is innovative, as identified in the analysis of the results, and as being in its infancy requires major advances. The coating system by using zinc as a sacrificial anode need further improvements, either by changing the net charge of the ACF or by changing the zinc surface to avoid or limit its dissolution. When aiming for local drug delivery systems, the drug release and form of release is crucial for the success of the implanted material. A deep understanding of this behavior is still missing, and its correlation with the initial drug design is essential for the success of this unexplored strategy.

F Bibliography

1. Seebach E, Kubatzky KF. Chronic Implant-Related Bone Infections-Can Immune Modulation be a Therapeutic Strategy? Frontiers in Immunology. 2019;10.
2. Rho JY, Kuhn-Spearing L, Zioupos P. Mechanical properties and the hierarchical structure of bone. Medical Engineering & Physics. 1998;20(2):92-102.
3. Piaia L, Salmoria GV, Hotza D. Additive Manufactured Nanocomposites for Bone Tissue Engineering Applications: an Overview. Materials Research-Ibero-American Journal of Materials. 2020;23(1).
4. Willie BM, Petersen A, Schmidt-Bleek K, Cipitria A, Mehta M, Strube P, et al. Designing biomimetic scaffolds for bone regeneration: why aim for a copy of mature tissue properties if nature uses a different approach? Soft Matter. 2010;6(20):4976-87.
5. Albrektsson T, Johansson C. Osteoinduction, osteoconduction and osseointegration. European Spine Journal. 2001;10:S96-S101.
6. What are Osteoblasts?. News Medical Life Sciences. (Acess on: https://www.news-medical.net/health/What-are-Osteoblasts.aspx, last acessed 10 July 2021)
7. Tabata Y. Biomaterial technology for tissue engineering applications. Journal of the Royal Society Interface. 2009;6:S311-S24.
8. Williams DF. TISSUE - BIOMATERIAL INTERACTIONS. Journal of Materials Science. 1987;22(10):3421-45.
9. L. Hirtzmann EC. La santé au Québec : les services de santé, les services sociaux, les sites Web2002.
10. Sneader W. The discovery of aspirin: a reappraisal. British Medical Journal. 2000;321(7276):1591-4.
11. Duarte M.T., Marins I.C.B., Quaresma S., André V. Mechanochemistry, a tool for improving drug physicochemical properties and delivery: salt formation and metal coordination. Acta Crystallographica a-Foundation and Advances. 2018;74:E135-E.
12. André V., Galego F., Martins M. Mechanochemical Assembly of Nalidixic Acid Bioinspired Metal-Organic Compounds and Complexes toward Improved Solubility. Crystal Growth & Design. 2018;18(4):2067-81.
13. André V., da Silva A.R.F., Fernandes A., Frade R., Garcia C., Rijo P., Mg- and Mn-MOFs Boost the Antibiotic Activity of Nalidixic Acid. Acs Applied Bio Materials. 2019;2(6):2347-54.
14. Barret R. Medicinal Chemistry: Fundamentals. edition s, editor: ISTE Press - Elsevier; 2018.
15. Thomas G. Fundamentals of Medicinal Chemistry: WILEY; 2003.
16. Ticehurst M.D., Marziano I. Integration of active pharmaceutical ingredient solid form selection and particle engineering into drug product design. Journal of Pharmacy and Pharmacology. 2015;67(6):782-802.
17. Al-Worafi Y.M. Drug Safety in Developing Countries. Academic Press.
18. Drug regulation. Pharmacology Education Project. (Acess on: https://www.pharmacologyeducation.org/clinical-pharmacology/drug-regulation, last acessed 20 July 2021)
19. Rägo L., Santoso B. Drug Regulation: History, Present and Future 1. Drug Benefits and Risks: International Textbook of Clinical Pharmacology. 2008 (2nd edition):65-76.
20. Almarsson Ö., Zaworotko M.J.. Crystal engineering of the composition of pharmaceutical phases. Do pharmaceutical co-crystals represent a new path to improved medicines? 2004.
21. About Antibiotic Resistance - Antibiotic/Antimicrobial Resistance. CDC. 2020. (Acess on: https://www.cdc.gov/drugresistance/biggest-threats.html, last acessed 7 July 2021)
22. DerSarkissian C. What you need to know about antibiotic resistance -- and how to protect yourself June 13, 2020 (Acess on: https://www.webmd.com/cold-and-flu/antibiotic-resistance, last acessed 8 July 2021)
23. Freire M.P., Song A.T.W., Oshiro I.C.V., Andraus W., D'Albuquerque L.A.C., Abdala E. Surgical site infection after liver transplantation in the era of multidrug-resistant bacteria: what new risks should be considered? Diagnostic Microbiology and Infectious Disease. 2021;99(1).
24. Ventola C. L. The antibiotic resistance crisis: part 1: causes and threats. P T. 2015;40(4):277-83.
25. Cohen L.L., Birch C.M., Cook D.L., Hedequist D.J., Karlin L.I., Emans J.B., Variability in Antibiotic Treatment of Pediatric Surgical Site Infection After Spinal Fusion at A Single Institution. Journal of Pediatric Orthopaedics. 2021;41(6):E380-E5.
26. Seaman S.J., Han E., Arora C., Kim J.H. Surgical site infections in gynecology: the latest evidence for prevention and management. Current Opinion in Obstetrics & Gynecology. 2021;33(4):296-304.
27. Llor C., Bjerrum L. Antimicrobial resistance: risk associated with antibiotic overuse and initiatives to reduce the problem.Ther Adv Drug Saf. 2014,(6):229-41.
28. (WHO) WHO. Antimicrobial Resistance: Global Report on Surveillance 2014: WHO Press, Geneva, Switzerland (Acess on:

https://apps.who.int/iris/bitstream/handle/10665/112647/WHO_HSE_PED_AIP_2014.2_eng.pdf, last acessed: 17 July 2021)

29. Vareil, M., Vinclair, C., Guerpillon,B., Leyssene,D., Jaouen,A., Alleman,L., Wille,H. Prolonged cefazolin course for treatment of methicillin susceptible staphylococcus species infections and the impact on the emergence of multidrug-resistant bacteria during cloxacillin shortage. Infectious Diseases Now.51(3):304-7.

30. Wise R., Hart T., Cars O., Streulens M., Helmuth R., Huovinen P.Antimicrobial resistance. Is a major threat to public health. BMJ. 1998 317(7159):609-10.

31. Khare T.,Mahalunkar S., Shriram V, Gosavi S, Kumar V. Embelin-loaded chitosan gold nanoparticles interact synergistically with ciprofloxacin by inhibiting efflux pumps in multidrug-resistant Pseudomonas aeruginosa and Escherichia coli. Environmental Research. 2021,111321.

32. O'neill, J. Tackling drug-resistant infections globally: final report and recommendations—the review on antimicrobial resistance. (Acess on: https://amr-review.org/sites/default/files/160518_Final%20paper_with%20cover.pdf, last acessed 10 June 2021)

33. Correia S., Poeta P., Hébraud M., Capelo J.L., Igrejas G. Mechanisms of quinolone action and resistance: where do we stand? Journal of medical microbiology. 2017;66(5).

34. Chu X., wnhg C., Liu W., Liang L., Gong K., Zhao C., Sun K. Quinoline and quinolone dimers and their biological activities: An overview,European Journal of Medicinal Chemistry - X-MOL. European Journal of Medicinal Chemistry. 2019;161:101-17.

35. Ahmed A, Daneshtalab M. Nonclassical Biological Activities of Quinolone Derivatives. Journal of pharmacy & pharmaceutical sciences : a publication of the Canadian Society for Pharmaceutical Sciences, Société canadienne des sciences pharmaceutiques. 2011;15:52-72.

36. Sissi C., Palumbo M. The Quinolone Family: From Antibacterial to Anticancer Agents. Current Medicinal Chemistry - Anti-Cancer Agents. 2003;3:439-50.

37. Pommier Y., Leo E., Zhang H., Marchand C. DNA Topoisomerases and Their Poisoning by Anticancer and Antibacterial Drugs. Chemistry & Biology. 2010;17(5):421-33.

38. Andersson M.I., MacGowan A.P. Development of the quinolones. Journal of Antimicrobial Chemotherapy. 2003;51:1-11.

39. Uivarosi V. Metal Complexes of Quinolone Antibiotics and Their Applications: An Update. Molecules. 2013;18(9):11153-97.

40. Zhang G.F., Zhang S., Pan B.F., Liu X.F., Feng L.S. 4-Quinolone derivatives and their activities against Gram positive pathogens. European Journal of Medicinal Chemistry. 2018;143:710-23.

41. Ball P. Quinolone generations: natural history or natural selection? Journal of Antimicrobial Chemotherapy. 2021;46;17-24.

42. Sousa I., Claro V., Pereira J.L., Amaral A.L., Cunha-Silva L., de Castro B. Synthesis, characterization and antibacterial studies of a copper(II) levofloxacin ternary complex. Journal of Inorganic Biochemistry. 2012;110:64-71.

43. Behrens N.B., Diaz G.M., Goodgame D.M.L. Metal complexes of the antibiotic nalidixic acid. Inorganica Chimica Acta. 1986;125(1):21-6.

44. Quaresma S., André V., Antunes A.M.M., Vilela S.M.F., Amariei G., Arenas-Vivo A., Novel Antibacterial Azelaic Acid BioMOFs. Crystal Growth & Design. 2020;20(1):370-82.

45. Alves P.C., Rijo P., Bravo C., Antunes A.M.M., André V. Bioactivity of Isostructural Hydrogen Bonding Frameworks Built from Pipemidic Acid Metal Complexes. Molecules. 2020;25(10).

46. Corona-Motolinia N.D., Martinez-Valencia B., Noriega L., Sanchez-Gaytan B.L., Mendez-Rojas M.A., Melendez F.J., Synthesis, Crystal Structure, and Computational Methods of Vanadium and Copper Compounds as Potential Drugs for Cancer Treatment. Molecules. 2020;25(20).

47. Quaresma S., Alves P.C., Rijo P., Duarte M.T., André V. Antimicrobial Activity of Pyrazinamide Coordination Frameworks Synthesized by Mechanochemistry. Molecules. 2021;26(7).

48. Abdolmaleki S., Ghadermazi M., Ashengroph M., Saffari A., Sabzkohi S.M. Cobalt (II), zirconium(IV), calcium(II) complexes with dipicolinic acid and imidazole derivatives: X-ray studies, thermal analyses, evaluation as in vitro antibacterial and cytotoxic agents. Inorganica Chimica Acta. 2018;480:70-82.

49. Yang L., Crans D.C., Miller S.M., la Cour A., Anderson O.P., Kaszynski P.M., Cobalt(II) and Cobalt(III) Dipicolinate Complexes: Solid State, Solution, and in Vivo Insulin-like Properties. Inorg Chem. 2002 ;41(19):4859-71.

50. Bravo C., Galego F., André V. Hydrogen bonding networks of nalidixic acid-copper(II) complexes. Crystengcomm. 2019;21(47):7199-203.

51. Braga D., Grepioni F., André V., Duarte M.T. Drug-containing coordination and hydrogen bonding networks obtained mechanochemically. Crystengcomm. 2009;11(12):2618-21.

52. André V., Hardeman A., Halasz I., Stein R.S., Jackson G.J., Reid D.G., Mechanosynthesis of the Metallodrug Bismuth Subsalicylate from Bi2O3 and Structure of Bismuth Salicylate without Auxiliary Organic Ligands. Angewandte Chemie-International Edition. 2011;50(34):7858-61.

53. Turel I. The interactions of metal ions with quinolone antibacterial agents. Coordination Chemistry Reviews. 2002;232:27-47.

54. Singh R. D.A., Masram D.T., Rathore D. Synthesis and Biological Activities of Selected Quinolone-Metal Complexes. Research Journal of Chemical Sciences. 2013;3(6):83-94.

55. Sha J., Peng J., Liu H., Chen J., Zhang, T. Asymmetrical Polar Modification of a Bivanadium-Capped Keggin POM by Multiple Cu−N Coordination Polymeric Chains. Inorg. Chem. 2007, 46, 26, 11183–11189.

56. Chunjiang L., Jingmei L., Fan T., Jingying C., Yujia L. Study of the first antibacterial agent pipemidic acid modifying Keggin polyoxometalate. Inorganic Chemistry Communications. 2011;14:1192-5.

57. Efthimiadou E.K., Sanakis, Y., Katsaros N, Karaliota A., Psomas G. Transition metal complexes with the quinolone antibacterial agent pipemidic acid: Synthesis, characterization and biological activity. Polyhedron. 2007;26(5):1148-58.

58. Kudelin A.I., Papathanasiou K., Isaeva V., Caro J., Salmi T., Kustov L.M.. Microwave-Assisted Synthesis, Characterization and Modeling of CPO-27-Mg Metal-Organic Framework for Drug Delivery. Molecules. 2021;26(2).

59. Trung T.K., Ramsahye N.A., Trens P., Tanchoux N., Serre C., Fajula F. Adsorption of C5-C9 hydrocarbons in microporous MOFs MIL-100(Cr) and MIL-101(Cr): A manometric study. Microporous and Mesoporous Materials. 2010;134(1-3):134-40.

60. Rosnes MH, Pato-Doldan B, Johnsen RE, Mundstock A, Caro J, Dietzel PDC. Role of the metal cation in the dehydration of the microporous metal-organic frameworks CPO-27-M. Microporous and Mesoporous Materials. 2020;309.

61. Usman K.A.S., Buenviaje S.C., Razal J.M., Conato M.T., PayawanJr. L.M. Synthesis and characterization of zinc adeninate metal-organic frameworks (bioMOF1) as potential anti-inflammatory drug delivery material. AIP Conference Proceedings 1958, 020018 (2018).

62. André V., Quaresma S. Bio-Inspired Metal-Organic Frameworks in the Pharmaceutical World: A Brief Review, Metal-Organic Frameworks, IntechOpen,2016.

63. Quaresma S., Andre V., Antunes A.M.M., Cunha-Silva L., Duarte M.T. Gabapentin Coordination Networks: Mechanochemical Synthesis and Behavior under Shelf Conditions. Crystal Growth & Design. 2013;13(11):5007-17.

64. André V., Shemchuk O., Grepioni F., Braga D., Duarte M.T. "Expanding the Pool of Multicomponent Crystal Forms of the Antibiotic 4-Aminosalicylic Acid: The Influence of Crystallization Conditions" on Publons. Crystal Growth & Design. 2017;17(12):65417–642.

65. Hu J.H., Johnston K.P., Williams R.O. Nanoparticle engineering processes for enhancing the dissolution rates of poorly water soluble drugs. Drug Development and Industrial Pharmacy. 2004;30(3):233-45.

66. Costa P., Manuel J., Lobo S. Modeling and comparison of dissolution profiles. European Journal of Pharmaceutical Sciences. 2001;13(2):123-33.

67. Salehi S., Moghaddam S.M.M., Tarin M., Saljooghi. A.S. Pharmaceutical Nickel(II) Chelation Properties of 3-Hydroxyflaven, Deferiprone and Maltol Metal Chelators: A Density Functional Study. Physical Chemistry Research. 2020;8.

68. Tran Q.H., Doan T.T. A novel study on curcumin metal complexes: solubility improvement, bioactivity, and trial burn wound treatment in rats. New Journal of Chemistry. 2020;44(30):13036-45.

69. Hirai K., Ito A., Abe Y., Suzue S., Irikura T., Inoue M. Comparative Activities of AM-715 and Pipemidic and Nalidixic Acids Against Experimentally Induced Systemic and Urinary Tract Infections. Antimicrobial Agents and Chemotherapy. 1981;19(1):188-9.

70. Salicylic acid 2021. PubChem. (Acess on: https://www.ncbi.nlm.nih.gov/pubmed/, last acessed 14 July 2021)

71. Nicotinic Acid Oral: Uses, Side Effects, Interactions, Pictures, Warnings & Dosing - WebMD (Acess on: https://www.webmd.com/drugs/2/drug-6142/nicotinic-acid-oral/details, last acessed 14 July 2021).

72. Chen W.T. Two Nd-Zn and Sm-Zn Isonicotinic/Nicotinic Acid Complexes. Acta Chimica Slovenica. 2011;58(1):144-50.

73. Konno K., Kurzmann R., Bird K.T., Sbarra A. Differentiation of human tubercle bacilli from atypical acid-fast bacilli. I. Niacin production of human tubercle bacilli and atypical acid-fast bacilli. American Review of Tuberculosis and Pulmonary Diseases. 1958;77(4):669-74.

74. Sameer R. Paital NBD. Calcium phosphate coatings for bio-implant applications: Materials, performance factors, and methodologies. Materials Science and Engineering. 2009;66(1-3):1-70.

75. Weaver C.M., Peacock M. Calcium. Advances in Nutrition. 2011:2(3)

76. Chen P., Bornhorst J., Aschner M. Manganese metabolism in humans. Frontiers in Bioscience-Landmark. 2018;23:1655-79.

77. Stock N., Biswas S. Synthesis of Metal-Organic Frameworks (MOFs): Routes to Various MOF Topologies, Morphologies, and Composites. Chemical Reviews. 2012;112(2):933-69.

78. Friščić T. New opportunities for materials synthesis using mechanochemistry. Journal of Materials Chemistry. 2010;20(36):7599-605.

79. Friščić T. Supramolecular concepts and new techniques in mechanochemistry: cocrystals, cages, rotaxanes, open metal-organic frameworks. Chemical Society Reviews. 2012;41(9):3493-510.

80. James S.L., Adams C.J., Bolm C., Braga D., Collier P., Friščić T., Mechanochemistry: opportunities for new and cleaner synthesis. Chemical Society Reviews. 2012;41(1):413-47.

81. Titi H.M., Do J.L., Howarth A.J., Nagapudi K., Friščić T. Simple, scalable mechanosynthesis of metal-organic frameworks using liquid-assisted resonant acoustic mixing (LA-RAM). Chemical Science. 2020;11(29):7578-84.

82. Friščić T., Mottillo C., Titi H.M. Mechanochemistry for Synthesis. Angewandte Chemie-International Edition. 2020;59(3):1018-29.

83. Hasa D., Carlino E., Jones W. Polymer-Assisted Grinding, a Versatile Method for Polymorph Control of Cocrystallization. Crystal Growth & Design. 2016;16(3):1772-9.

84. Hasa D., Rauber G. S., Voinovich D., Jones W. Cocrystal Formation through Mechanochemistry: from Neat and Liquid-Assisted Grinding to Polymer-Assisted Grinding. Angewandte Chemie (International ed in English). 2015;54(25).

85. Lomovskiy I., Bychkov A., Lomovsky O., Skripkina T. Mechanochemical and Size Reduction Machines for Biorefining. Molecules. 2020;25(22).

86. Fenton O.S., Olafson K.N., Pillai P.S., Mitchell M.J., Langer R. Advances in Biomaterials for Drug Delivery. Advanced Materials. 2018;30(29).

87. Pang X., Yang X.Y., Zhai G.X. Polymer-drug conjugates: recent progress on administration routes. Expert Opinion on Drug Delivery. 2014;11(7):1075-86.

88. Alqahtani M.S., Kazi M., Alsenaidy M.A., Ahmad M.Z. Advances in Oral Drug Delivery. Frontiers in Pharmacology. 2021;12.

89. Hoffman A., Stepensky D. Pharmacodynamic aspects of modes of drug administration for optimization of drug therapy. Critical Reviews in Therapeutic Drug Carrier Systems. 1999;16(6):571-639.

90. Choudhury H., Gorain B., Chatterjee B., Mandal U.K., Sengupta P., Tekade R.K. Pharmacokinetic and Pharmacodynamic Features of Nanoemulsion Following Oral, Intravenous, Topical and Nasal Route. Current Pharmaceutical Design. 2017;23(17):2504-31.

91. Chen A., Shi Y., Yan Z.Q., Hao H.X., Zhang Y., Zhong J. Dosage Form Developments of Nanosuspension Drug Delivery System for Oral Administration Route. Current Pharmaceutical Design. 2015;21(29):4355-65.

92. Alabdulhafith M., Sampalli S. NFC-Based Framework for Checking the Five Rights of Medication Administration. 5th International Conference on Emerging Ubiquitous Systems and Pervasive Networks / the 4th International Conference on Current and Future Trends of Information and Communication Technologies in Healthcare / Affiliated Workshops. 2014;37:434-8.

93. Vonrecum A.F., Laberge M. Educational goals for biomaterials science and engineering: prospective view. Journal of Applied Biomaterials. 1995;6(2):137-44.

94. Ratner B.D., Bryant S.J. Biomaterials: Where we have been and where we are going. Annual Review of Biomedical Engineering. 2004;6:41-75.

95. Ahirwar H., Zhou Y.B., Mahapatra C., Ramakrishna S., Kumar P., Nanda H.S. Materials for Orthopedic Bioimplants: Modulating Degradation and Surface Modification Using Integrated Nanomaterials. Coatings. 2020;10(3).

96. Liu G., He Y.H., Liu P.C., Chen Z., Chen X.L., Wan L. Development of Bioimplants with 2D, 3D, and 4D Additive Manufacturing Materials. Engineering. 2020;6(11):1232-43.

97. Hench L.L., Polak J.M. Third-generation biomedical materials. Science. 2002;295(5557):1014.

98. Maurus P.B., Kaeding C.C. Bioabsorbable implant material review. Operative Techniques in Sports Medicine. 2004;12(3):158-60.

99. Isyar M., Yilmaz I., Nusran G., Guler O., Yalcin S., Mahirogullari M. Safety of bioabsorbable implants in vitro. Bmc Surgery. 2015;15.

100. Zamora R., Jackson A., Seligson D. Correct techniques for the use of bioabsorbable implants in orthopaedic trauma. Current Orthopaedic Practice. 2016;27(4):469-73.

101. Godbey W.T., Atala A. In vitro systems for tissue engineering. In: Sipe JD, Kelley CA, McNicol LA, editors. Reparative Medicine: Growing Tissues and Organs. Annals of the New York Academy of Sciences. 9612002. p. 10-26.

102. Patrick C.W. Breast tissue engineering. Annual Review of Biomedical Engineering. 2004;6:109-30.

103. Moravej M., Mantovani D. Biodegradable Metals for Cardiovascular Stent Application: Interests and New Opportunities. International Journal of Molecular Sciences. 2011;12(7):4250-70.

104. Nasution A.K. H.H. Degradable Biomaterials for Temporary Medical Implants. Biomaterials and Medical Devices. 2016;58:127-60.

105. Bottoni C.R., DeBerardino T.M., Fester W., Mitchell D., Penrod B.J. An intra-articular bioabsorbable interference screw mimicking an acute meniscal tear 8 months after an anterior cruciate ligament reconstruction. Arthroscopy. 2000;16(4):395-8.

106. Cummins C.A., Strickland S., Appleyard R.C., Szomor Z.L., Marshall J., Murrell G.A.C. Rotator cuff repair with bioabsorbable screws: An in vivo and ex vivo investigation. Arthroscopy-the Journal of Arthroscopic and Related Surgery. 2003;19(3):239-48.

107. Prakasam M., Locs J., Salma-Ancane K., Loca D., Largeteau A., Berzina-Cimdina L. Biodegradable Materials and Metallic Implants-A Review. Journal of Functional Biomaterials. 2017;8(4).

108. Su Y.C., Cockerill I., Wang Y.D., Qin Y.X., Chang L.Q., Zheng Y.F. Zinc-Based Biomaterials for Regeneration and Therapy. Trends in Biotechnology. 2019;37(4):428-41.

109. Zinc - Crystal Structure 2020. Material Properties. (Acess on: https://material-properties.org/Zinc-properties-applications-price-production/, last acess 2 Jan 2021)

110. Gotman I. Characteristics of metals used in implants. Journal of Endourology. 1997;11(6):383-9.

111. Li X.D., Li Y.F., Peng S.C., Ye B., Lin W., Hu J. Effect of zinc ions on improving implant fixation in osteoporotic bone. Connective Tissue Research. 2013;54(4-5):290-6.

112. Bowen P.K., Drelich J., Goldman J. Zinc Exhibits Ideal Physiological Corrosion Behavior for Bioabsorbable Stents. Advanced Materials. 2013;25(18):2577-82.

113. Alves M.M., Prošek T., Santos C.F., Montemor M.F. Evolution of the in vitro degradation of Zn–Mg alloys under simulated physiological conditions. The Royal Society of Chemistry.2017., 7 (45).7, 28224.

114. Yang H.T., Wang C., Liu C.Q., Chen H.W., Wu Y.F., Han J.T. Evolution of the degradation mechanism of pure zinc stent in the one-year study of rabbit abdominal aorta model. Biomaterials. 2017;145:92-105.

115. Liu L.J., Meng Y., Dong C.F., Yan Y., Volinsky A.A., Wang L.N. Initial formation of corrosion products on pure zinc in simulated body fluid. Journal of Materials Science & Technology. 2018;34(12):2271-82.

116. Alves M.M., Cunha D.V., Santos C.F., Mira N.P., Montemor M.F. In vitro corrosion behaviour and anti-Candida spp. activity of Zn coated with ZnO-nanostructured 'Anastacia' flowers. Journal of Materials Chemistry B. 2016;4(27):4754-61.

117. Alves M.M., Santos C.F., Carmezim M.J., Montemor M.F. Nanostructured 'Anastacia' flowers for Zn coating by electrodepositing ZnO at room temperature. Applied Surface Science. 2015;332:152-8.

118. Alves M.M., Mil-Homens D., Pinto S., Santos C.F., Montemor M.F. Antagonist biocompatibilities of Zn-based materials functionalized with physiological active metal oxides. Colloids and Surfaces B-Biointerfaces. 2020;191.

119. Alves M.M., Marques L.M., Nogueira I., Santos C.F., Salazar S.B., Eugenio S. In silico, in vitro and antifungal activity of the surface layers formed on zinc during this biomaterial degradation. Applied Surface Science. 2018;447:401-7.

120. Bowen P.K., Shearier E.R., Zhao S., Guillory R.J., Zhao F., Goldman J. Biodegradable Metals for Cardiovascular Stents: from Clinical Concerns to Recent Zn-Alloys. Advanced Healthcare Materials. 2016;5(10):1121-40.

121. Little P.J., Bhattacharya R., Moreyra A.E., Korichneva I.L. Zinc and cardiovascular disease. Nutrition. 2010;26(11-12):1050-7.

122. Pluhator M.M., Thomson A.B.R., Fedorak R.N. Clinical aspects of trace elements: Zinc in human nutrition - Zinc deficiency and toxicity. Canadian Journal of Gastroenterology. 1996;10(2):97-103.

123. Kaddachi Z., Belhi M., Ben Karoui M., Gharbi R. Design and Development of Spin Coating System. 17th International Conference on Sciences and Techniques of Automatic Control and Computer Engineering; 2016. 19-21.

124. Takahashi Y., Okada S., Tahar R.B.H., Nakano K., Ban T., Ohya Y. Dip-coating of ITO films. Journal of Non-Crystalline Solids. 1997;218:129-34.

125. Hammond P.T.Building biomedical materials layer-by-layer.Materials Today. 2012 (15), 5, 196-206.

126. Sweeney T., Whatmore R.W.. Electrophoretic deposition of PZT ceramic films. Isaf '96 - Proceedings of the Tenth Ieee International Symposium on Applications of Ferroelectrics, Vols 1 - 2. 1996:193-6.

127. Jelinek , Trtik V., Jastrabik L.. Pulsed laser deposition of thin films. NATO Advenced Science Isntitute Series, Sub-series 3, High Technology. 1997, 16, 215-31.

128. Kawakami R., Ito K., Sato Y., Mori Y., Adachi M., Yoshikado S. Evaluation of TiO2 Nanoparticle Thin Films Prepared by Electrophoresis Deposition. Electroceramics in Japan Xiv. 2011;485:165-8.

129. Zdansky K., Zavadil J., Kacerovsky P., Lorincik J., Vanis J., Kostka F. Electrophoresis deposition of metal nanoparticles with reverse micelles onto InP. International Journal of Materials Research. 2009;100(9):1234-8.

130. Etter M., Dinnebier R.E. A Century of Powder Diffraction: a Brief History. Zeitschrift Fur Anorganische Und Allgemeine Chemie. 2014;640(15):3015-28.

131. BraggsLaw 2021. University Carleton (Acess on: https://serc.carleton.edu/research_education/geochemsheets/BraggsLaw.html, last acessed 10 Mar 2021)

earn Crystal Lattice Unit Cells meaning, concepts, formulas through Study Material.

134. Learn Crystal Lattice Unit Cells meaning, concepts, formulas through Study Material. Embibe 2021 (Acess on: https://www.embibe.com/study/crystal-lattice-unit-cells-concept?entity_code=KTSD06, last acessed 15 May 2021)

133. Brittain H.B. Polymorphism in Pharmaceutical Solids. Drugs and Pharmaceutical Sicences, 1999, 192.

134. X-ray Diffraction. Pruffle. (Acess on: http://pruffle.mit.edu/atomiccontrol/education/xray/xray_diff.php, last acessed 115 Jul 2021)

135. Energy-dispersive detector (EDS) 2021. Unieversity Carleton. (Acess on: https://serc.carleton.edu/research_education/geochemsheets/eds.html, last acessed 18 Jul 2021)

136. Dominguez-Benetton X, Sevda S, Vanbroekhoven K, Pant D. The accurate use of impedance analysis for the study of microbial electrochemical systems. Chemical Society Reviews. 2012;41(21):7228-46.

137. Harrington D.A., Van den Driessche P. Mechanism and equivalent circuits in electrochemical impedance spectroscopy. Electrochimica Acta. 2011;56(23):8005-13.

138. Basics of EIS: Electrochemical Research-Impedance. Gamry. (Acess on: https://www.gamry.com/application-notes/EIS/basics-of-electrochemical-impedance-spectroscopy/, acessed on: 20 Jul 2021)

139. Lukacs Z., Kristof T.. A generalized model of the equivalent circuits in the electrochemical impedance spectroscopy. Electrochimica Acta. 2020;363.

140. Kokudo T., Takama H. How useful is SBF in predicting in vivo bone bioactivity? Biomaterials. 2006;27(15).

141. Kokubo T., Kushitani H., Sakka S., Kitsugi T., Yamamuro T.. Solutions able to reproduce in vivo surface-structure changes in bioactive glass-ceramic A-W. Journal of biomedical materials research. 1990;24(6).

142. Bruker AXS: SAINT+, release 6.22. Bruker Analytical Systems: Madison,WI. 2005.

143. Bruker AXS:SADABS. Bruker Analytical Systems: Madison,WI. 2005.

144. Sheldrick GM. A short history of SHELX. Acta Crystallographica Section A. 2008;64:112-22.

145. Farrugia LJ. WinGX - Version 1.80.05. J Appl Cryst. 1999;32:837-8.

146. Macrae CF, Bruno IJ, Chisholm JA, Edgington PR, McCabe P, Pidcock E, et al. Mercury CSD 2.0 - new features for the visualization and investigation of crystal structures. Journal of Applied Crystallography. 2008;41:466-70.

147. Spek A.L. Single-crystal structure validation with the program PLATON. Journal of Applied Crystallography. 2003;36:7-13.

148. Siopa F., Figueiredo T., Frade R.F.M., Neto I., Meirinhos A., Reis C.P. Choline-Based Ionic Liquids: Improvement of Antimicrobial Activity. Chemistryselect. 2016;1(18):5909-16.

149. Methods for dilution Antimicrobial susceptibility tests for bacteria that grow aerobically. Clinical and Laboratory Standards Institute. 2018. (acess on: https://clsi.org/media/1928/m07ed11_sample.pdf, last acessed 5 Jul 2021)

150. Chang C.K., Zhu R.Y., Mao D.L., Wu J.S., Ding C.X.. Characterization of plasma sprayed hydroxyapatite coating. Journal of Inorganic Materials. 2000;15(5):952-6.

151. Andronescu E., Stefan E., Dinu E., Ghitulica C. Hydroxyapatite synthesis. Euro Ceramics Vii, Pt 1-3. 2002;206-2:1595-8.

152. Trommer R.M., Santos L.A., Bergmann C.P. Alternative technique for hydroxyapatite coatings. Surface & Coatings Technology. 2007;201(24):9587-93.

153. Pang X., Zhitomirsky I. Electrophoretic deposition of composite hydroxyapatite-chitosan coatings. Materials Characterization. 2007;58(4):339-48.

154. Jayabalan M, Shalumon KT, Mitha MK, Ganesan K, Epple M. The effect of radiation processing and filler morphology on the biomechanical stability of a thermoset polyester composite. Biomedical Materials. 2010;5(2).

155. Manafi S.A., Yazdani B., Rahimiopour M.R., Sadrnezhaad S.K., Amin M.H., Razavi M. Synthesis of nano-hydroxyapatite under a sonochemical/hydrothermal condition. Biomedical Materials. 2008;3(2).

156. Calasans-Maia MD, de Melo B.R., Alves A., Resende R.F.D., Louro R.S., Sartoretto S.C. Cytocompatibility and biocompatibility of nanostructured carbonated hydroxyapatite spheres for bone repair. Journal of Applied Oral Science. 2015;23(6):599-608.